

Quantum Latent Gauge and Coherence Selective Forces

Ridha Horchani (email: horchani@squ.edu.om)¹

¹*Department of Physics, College of Science, Sultan Qaboos University,
P.O. Box 36, P.C. 123, Al-Khod, Muscat, Sultanate of Oman*

We propose a hidden $U(1)$ gauge interaction that couples exclusively to quantum coherence in massive systems. The central innovation is a conserved coherence current operator constructed from the Noether mass current via operator-level coarse-graining. This current vanishes for classical matter distributions but is nonzero for spatial superpositions and entangled states, yielding a gauge interaction that is dormant in classical regimes but activated by quantum coherence.

The framework predicts three distinctive signatures: (i) interferometric phase shifts scaling linearly with fringe visibility, (ii) decoherence rates with characteristic m^2 scaling and spatial dependence distinct from collapse models, and (iii) entanglement-selective forces between distant massive qubits. The theory maintains full gauge invariance, causality, and positive time evolution.

We show that state-of-the-art atom interferometers and levitated nanoparticles can place first constraints on this interaction class, complementary to classical fifth-force searches. This approach provides a novel theoretical framework for probing coherence-selective fundamental interactions and their potential role in the quantum-classical transition.

To make this more concrete, we also spell out a simple benchmark latent-field model and work out, in detail, how a representative large-momentum-transfer atom interferometer constrains the corresponding coupling strength.

I. INTRODUCTION

The emergence of classical behavior from underlying quantum dynamics represents one of the most profound open questions in fundamental physics [1, 2]. This question dates back to the earliest foundations of quantum theory [3] and continues to motivate both theoretical and experimental research into the quantum-classical transition [4]. In contemporary understanding, the macroscopically classical world is typically explained through environmental decoherence, where uncontrolled entanglement with environmental degrees of freedom suppresses interference between macroscopically distinct outcomes [5, 6]. While this framework remains compatible with standard quantum mechanics, it leaves conceptual space for additional, potentially fundamental structure that might govern the quantum-classical transition.

Complementary research directions have pursued explicit modifications to quantum theory, notably through dynamical collapse models. The paradigmatic Continuous Spontaneous Localization (CSL) model [7, 8] introduces a stochastic classical field coupled to mass density, driving spatial superpositions toward localized states with rates that scale with system mass. These models predict novel decoherence channels and have motivated extensive experimental programs with massive quantum superpositions [9, 10], including groundbreaking matter-wave interferometry with increasingly massive objects [11, 12]. Concurrently, extensive searches for new fundamental interactions—so-called “fifth forces”—have systematically probed deviations from Newtonian gravity and electromagnetism across multiple length scales using macroscopic and astrophysical probes [13–15]. However, these experimental tests predominantly involve classical sources and consequently remain largely insensitive to interactions that activate exclusively in the presence of quantum co-

herence. This limitation is particularly relevant given recent proposals that gravity itself may exhibit quantum features that are only apparent in coherent superpositions [16, 17].

In this work, we explore a qualitatively different possibility: the existence of a hidden gauge interaction that is fundamentally coherence-selective. We construct a hidden $U(1)$ gauge field A_μ that couples not to the total mass density, but to a coherence current operator $\hat{J}_{(\text{coh})}^\mu(x)$ defined within the matter Hilbert space. This coherence current is engineered to satisfy several essential properties. First, it is exactly conserved, with $\partial_\mu \hat{J}_{(\text{coh})}^\mu(x) = 0$ as an operator identity. Second, it transforms covariantly under the local phase symmetry defining the Noether mass current. Third, its expectation value vanishes for density matrices diagonal in position at a given coarse-graining scale, corresponding to classical probability distributions. Finally, it exhibits nonzero expectation for spatial superpositions and entangled states, thereby capturing the interference contributions to the mass current.

The resulting interaction is intrinsically latent: it remains invisible to classical matter, thereby evading conventional fifth-force constraints, yet becomes activated in the presence of quantum coherence. This approach draws inspiration from recent developments in understanding quantum reference frames [18] and the role of coherence in gravitational interactions [19, 20], while introducing a novel gauge-theoretic perspective on the quantum-classical divide.

A compact visual summary of this mechanism is shown in Fig. 1: panel (a) depicts a single, smooth mass distribution that is effectively classical and therefore sources only the coarse-grained current, leaving the latent gauge field in a uniform, dormant configuration with straight field lines. Panel (b) illustrates a spatial superposition with two well-separated lobes and interference structure;

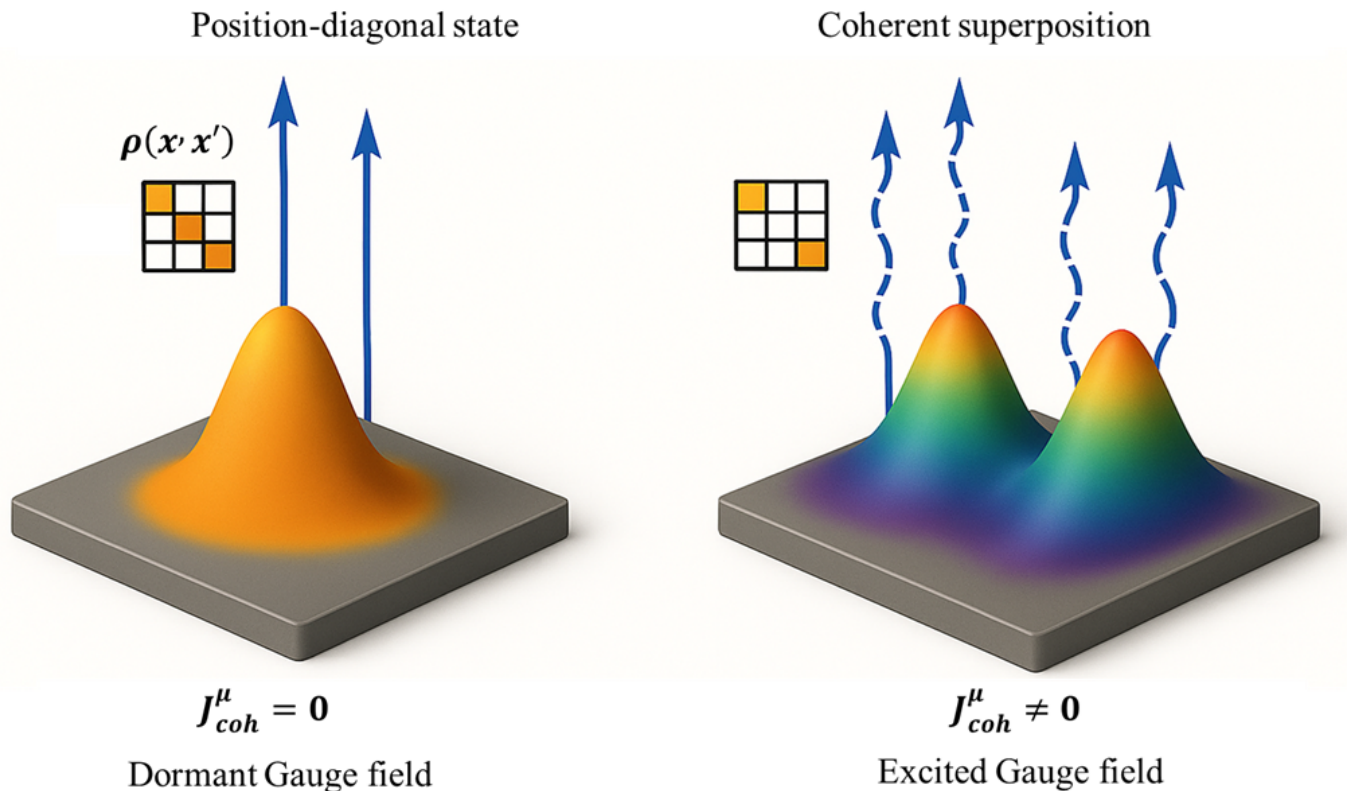


FIG. 1. Conceptual illustration of the Quantum Latent Gauge (QLG) interaction. Right panel shows a single, smooth mass distribution that is effectively classical: it sources only the coarse-grained (classical) mass current and leaves the latent gauge field A_μ in a uniform, dormant configuration, indicated by straight field lines. Left panel shows a spatially coherent superposition with two separated lobes and interference structure: the off-diagonal elements of the density matrix generate a non-zero coherence current, which “activates” the QLG field and leads to a distorted, wavy field pattern. Classical mixtures with the same coarse-grained mass profile as in panel (b) would not excite the latent field, underscoring the coherence-selective nature of the coupling.

in this case the off-diagonal density-matrix elements generate a non-vanishing coherence current, which in turn excites and distorts the QLG field, represented by the wavy field lines emanating from the coherent mass profile.

The phenomenology emerging from such a Quantum Latent Gauge interaction is remarkably rich. The coherence current sourcing A_μ induces interferometric phase shifts proportional to fringe visibility \mathcal{V} that vanish when which-path information destroys coherence. Furthermore, tracing out the A_μ field generates decoherence channels whose rates scale with mass and superposition size in a manner dictated by field correlators and the coarse-graining scale, exhibiting structural distinctions from the Gaussian kernels characteristic of CSL models. Additionally, the coherence current mediates effective, entanglement-selective interactions between distant massive qubits that vanish for classically correlated mixtures but remain nonzero for entangled states, reminiscent of coherence-based phenomena in quantum information theory.

In what follows we treat the coarse-graining scale Λ as a phenomenological parameter that encodes the spatial resolution at which mass distributions behave effectively

classical for the purposes of the latent interaction. We assume that Λ is universal for a given realization of the theory, while remaining agnostic as to whether it is ultimately fundamental (for instance of gravitational or Planckian origin) or emergent from some microscopic environmental or many-body mechanism. Different microscopic completions may thus realize different specific values of Λ , but the qualitative structure of the coherence-selective coupling is insensitive to this distinction.

It is also important to stress that the operator coarse-graining map we employ is not claimed to be mathematically unique: there exists a family of linear, completely positive, gauge-covariant maps that satisfy our axioms. In this sense the present construction should be viewed as a representative member of a broader class of Quantum Latent Gauge-like models, all of which share the key physical feature that purely position-diagonal states do not source the interaction, while coherent superpositions and entangled states do.

The remainder of this paper develops these ideas systematically. Section II establishes the theoretical framework, defining the operator-level coarse-graining that splits the

mass current into classical and coherence components and constructing the gauge-invariant action. Section III derives the leading experimental signatures in interferometers, massive superpositions, and entanglement experiments. Section IV estimates experimental constraints from current and near-future platforms. In Section V, we discuss theoretical consistency requirements, including gauge invariance, causality, positivity of the reduced dynamics, and relations to CSL and stochastic-gravity models. We conclude with an outlook in Section VI, while technical derivations are provided in the appendices.

For readers seeking an intuitive picture, we note already here that in the single-particle, nonrelativistic limit the coherence current reduces to a coarse-grained “coherence density” built directly from the off-diagonal elements of the position-space density matrix; this limit is made explicit in Appendix E and provides a useful bridge between the abstract operator construction and familiar wavefunction-based intuition.

Throughout the theoretical development, we employ natural units with $\hbar = c = 1$, restoring SI units exclusively for numerical estimates and experimental bounds.

II. THEORETICAL FRAMEWORK

A. Gauge principle and mass current

We begin by promoting the proper-time phase symmetry of massive particles to a local gauge symmetry. For a nonrelativistic matter field $\psi(x)$ of mass m we consider local phase transformations

$$\psi(x) \rightarrow e^{igm\chi(x)}\psi(x), \quad A_\mu(x) \rightarrow A_\mu(x) - \partial_\mu\chi(x), \quad (1)$$

where g is a dimensionless coupling, $\chi(x)$ is a smooth function, and A_μ is the hidden gauge field. The corresponding covariant derivative reads

$$D_\mu\psi = (\partial_\mu + igmA_\mu)\psi. \quad (2)$$

In the nonrelativistic regime the matter Lagrangian can be written as

$$\mathcal{L}_\psi = \frac{i}{2} (\psi^\dagger D_t\psi - (D_t\psi)^\dagger\psi) - \frac{1}{2m} |\mathbf{D}\psi|^2 - V(\mathbf{x})\psi^\dagger\psi, \quad (3)$$

where V is an external potential. The hidden gauge field has the usual kinetic term

$$\mathcal{L}_A = -\frac{1}{4} F_{\mu\nu}F^{\mu\nu}, \quad F_{\mu\nu} = \partial_\mu A_\nu - \partial_\nu A_\mu. \quad (4)$$

The Lagrangian $\mathcal{L}_\psi + \mathcal{L}_A$ is invariant under Eq. (1).

Applying Noether’s theorem to the matter sector yields a conserved mass-current operator $\hat{J}^\mu(x)$, which in the nonrelativistic approximation takes the familiar form

$$\hat{J}^\mu(x) = (\hat{n}(x), \hat{\mathbf{J}}(x)), \quad (5)$$

$$\hat{n}(x) = \psi^\dagger(x)\psi(x), \quad (6)$$

$$\hat{\mathbf{J}}(x) = \frac{1}{2m} \left[\psi^\dagger(-i\nabla)\psi - ((-i\nabla)\psi)^\dagger\psi \right], \quad (7)$$

satisfying the operator identity

$$\partial_\mu \hat{J}^\mu(x) = 0, \quad (8)$$

provided the matter fields obey their equations of motion. The vector \hat{J}^μ transforms covariantly under the local symmetry generated by Eq. (1).

B. Operator-level coarse-grained classical current

Our goal is to decompose the full current into a “classical” part that depends only on position-diagonal density-matrix elements, and a “coherence” part that captures off-diagonal interference contributions. Crucially, we require this decomposition to be implemented at the operator level, so that both pieces are conserved and transform correctly under the gauge symmetry.

To this end, we introduce an operator coarse-graining superoperator

$$\mathcal{C}_\Lambda^{(\text{op})} : \hat{O} \mapsto \mathcal{C}_\Lambda^{(\text{op})}[\hat{O}], \quad (9)$$

defined in the position basis as

$$\mathcal{C}_\Lambda^{(\text{op})}[\hat{O}] = \int d^3x \Pi_x \hat{O} \Pi_x, \quad \Pi_x = \int d^3y f_\Lambda(\mathbf{y}-\mathbf{x}) |y\rangle\langle y|. \quad (10)$$

Here f_Λ is a real, normalized smearing kernel of width $\sim \Lambda^{-1}$, and $|x\rangle$ denotes approximate position eigenstates. The projectors Π_x are positive and resolve the identity, $\int d^3x \Pi_x = \mathbb{I}$. The map $\mathcal{C}_\Lambda^{(\text{op})}$ thus removes off-diagonal elements of \hat{O} in the position basis on scales larger than Λ^{-1} , while preserving its Hermiticity.

From a structural point of view, we restrict attention to coarse-graining maps that are linear, completely positive, and trace-preserving on the space of bounded operators, and that commute with the unitary representation of the hidden $U(1)$ symmetry. These conditions ensure that $\mathcal{C}_\Lambda^{(\text{op})}$ can be regarded as an admissible “quantum channel” acting on operators, and they guarantee that the decomposition of the current into classical and coherent parts is both physically interpretable and compatible with the gauge structure of the theory.

We then define the classical current operator and the coherence current operator as

$$\hat{J}_{(\text{cl})}^\mu(x) = \mathcal{C}_\Lambda^{(\text{op})}[\hat{J}^\mu(x)], \quad (11)$$

$$\hat{J}_{(\text{coh})}^\mu(x) = \hat{J}^\mu(x) - \hat{J}_{(\text{cl})}^\mu(x). \quad (12)$$

Because $\mathcal{C}_\Lambda^{(\text{op})}$ is defined in terms of position projectors and commutes with multiplication by smooth c-number functions of x , it commutes with the derivative operator acting on the explicit x -dependence of $\hat{J}^\mu(x)$. Applying ∂_μ to Eq. (11) and using Eq. (8), we obtain

$$\partial_\mu \hat{J}_{(\text{cl})}^\mu(x) = \mathcal{C}_\Lambda^{(\text{op})}[\partial_\mu \hat{J}^\mu(x)] = 0. \quad (13)$$

It then follows from Eq. (12) that

$$\partial_\mu \hat{J}_{(\text{coh})}^\mu(x) = 0. \quad (14)$$

Thus both currents are exactly conserved operators.

Gauge covariance: The Noether current \hat{J}^μ is obtained from a gauge-invariant Lagrangian and therefore transforms covariantly under Eq. (1). The coarse-graining map $\mathcal{C}_\Lambda^{(\text{op})}$ is built from position projectors Π_x and is independent of the local phase of the matter field; it thus commutes with the unitary representation of Eq. (1). Hence both $\hat{J}_{(\text{cl})}^\mu$ and $\hat{J}_{(\text{coh})}^\mu$ inherit the same transformation properties as \hat{J}^μ , and in particular remain suitable sources for a gauge theory.

Vanishing expectation for classical mixtures: Consider a density matrix that is diagonal in the (smeared) position basis,

$$\rho_{\text{cl}} = \int d^3x p(x) |x\rangle\langle x|, \quad p(x) \geq 0, \quad \int d^3x p(x) = 1. \quad (15)$$

Using Eq. (10), we find that for such a state

$$\mathcal{C}_\Lambda^{(\text{op})}[\hat{O}] \rho_{\text{cl}} = \hat{O} \rho_{\text{cl}}, \quad (16)$$

whenever \hat{O} acts only on the position-diagonal components at the resolution set by f_Λ . Applying this to $\hat{J}^\mu(x)$ yields

$$\begin{aligned} \text{Tr} [\rho_{\text{cl}} \hat{J}_{(\text{coh})}^\mu(x)] &= \text{Tr} [\rho_{\text{cl}} \hat{J}^\mu(x)] - \text{Tr} [\rho_{\text{cl}} \hat{J}_{(\text{cl})}^\mu(x)] \\ &= \text{Tr} [\rho_{\text{cl}} \hat{J}^\mu(x)] - \text{Tr} [\rho_{\text{cl}} \mathcal{C}_\Lambda^{(\text{op})}[\hat{J}^\mu(x)]] = 0. \end{aligned} \quad (17)$$

Thus pure classical mixtures (at resolution Λ^{-1}) do not source the coherence current.

Sensitivity to spatial coherence: For a pure superposition of two well-separated localized states,

$$|\psi\rangle = \alpha |x_1\rangle + \beta |x_2\rangle, \quad |\mathbf{x}_1 - \mathbf{x}_2| \gg \Lambda^{-1}, \quad (18)$$

the full current \hat{J}^μ contains both diagonal contributions (corresponding to the classical probability of being near x_1 or x_2) and off-diagonal interference terms. The coarse-graining map $\mathcal{C}_\Lambda^{(\text{op})}$ removes the off-diagonal elements in the position basis, so that $\hat{J}_{(\text{cl})}^\mu$ retains only the classical parts, while $\hat{J}_{(\text{coh})}^\mu$ isolates the interference contributions. The expectation value $\text{Tr} [\rho \hat{J}_{(\text{coh})}^\mu(x)]$ is thus proportional to the off-diagonal element of ρ in the $\{|x_1\rangle, |x_2\rangle\}$ subspace and vanishes when the superposition is decohered by an external environment.

Physically, one may think of $\mathcal{C}_\Lambda^{(\text{op})}$ as implementing the coarse spatial resolution with which any realistic macroscopic apparatus would probe the mass distribution: at that resolution only position-diagonal information survives as a ‘‘classical’’ source, whereas finer interference fringes are encoded solely in $\hat{J}_{(\text{coh})}^\mu$. The decomposition therefore does not introduce an additional measurement postulate, but rather formalizes within the operator algebra the distinction between coarse-grained densities and genuinely quantum-coherent structure.

C. Illustrative example: two-packet superposition vs classical mixture

To make the abstract operator construction more concrete, consider a single nonrelativistic particle in one spatial dimension, prepared in a superposition of two spatially separated wave packets. For definiteness, let

$$|\psi_{\text{sup}}\rangle = c_L |\phi_L\rangle + c_R |\phi_R\rangle, \quad |c_L|^2 + |c_R|^2 = 1, \quad (19)$$

where $|\phi_{L,R}\rangle$ are normalized Gaussian wave packets centered at $x_{L,R}$ with spatial width ℓ ,

$$\phi_L(x) = \frac{1}{(2\pi\ell^2)^{1/4}} \exp\left(-\frac{(x-x_L)^2}{4\ell^2}\right) \quad (20)$$

$$\phi_R(x) = \frac{1}{(2\pi\ell^2)^{1/4}} \exp\left(-\frac{(x-x_R)^2}{4\ell^2}\right) \quad (21)$$

with $|x_R - x_L| \gg \ell$ so that the two packets are well separated on the microscopic scale. We compare this genuinely coherent state with the classical mixture

$$\rho_{\text{cl}} = |c_L|^2 |\phi_L\rangle\langle\phi_L| + |c_R|^2 |\phi_R\rangle\langle\phi_R|, \quad (22)$$

which has the same coarse-grained position density but no off-diagonal coherences between $|\phi_L\rangle$ and $|\phi_R\rangle$.

The full microscopic density matrices in the position basis read

$$\begin{aligned} \rho_{\text{sup}}(x, x') &= \psi_{\text{sup}}(x) \psi_{\text{sup}}^*(x') \\ &= |c_L|^2 \phi_L(x) \phi_L^*(x') + |c_R|^2 \phi_R(x) \phi_R^*(x') \\ &\quad + c_L c_R^* \phi_L(x) \phi_R^*(x') + c_R c_L^* \phi_R(x) \phi_L^*(x'), \end{aligned} \quad (23)$$

$$\rho_{\text{cl}}(x, x') = |c_L|^2 \phi_L(x) \phi_L^*(x') + |c_R|^2 \phi_R(x) \phi_R^*(x'). \quad (24)$$

The last two terms in $\rho_{\text{sup}}(x, x')$ are the genuine coherence contributions, which oscillate on the scale of the packet separation $|x_R - x_L|$ and are fully absent in ρ_{cl} .

Now apply the coarse-graining channel $\mathcal{C}_\Lambda^{(\text{op})}$ with a resolution scale Λ^{-1} chosen such that

$$\ell \ll \Lambda^{-1} \ll |x_R - x_L|. \quad (25)$$

In this regime, each of the localized packets is essentially pointlike at the coarse-grained resolution, whereas the interference fringes between ϕ_L and ϕ_R oscillate faster than the coarse-graining kernel and are partially averaged out. One finds that the *coarse-grained* density matrix elements become

$$[\mathcal{C}_\Lambda(\rho_{\text{sup}})](x, x') \simeq [\mathcal{C}_\Lambda(\rho_{\text{cl}})](x, x') + \mathcal{O}(\epsilon_\Lambda), \quad (26)$$

where ϵ_Λ is a small parameter that quantifies the residual sensitivity of \mathcal{C}_Λ to the long-wavelength part of the coherence terms. In particular, the position density

$n(x) = \rho(x, x)$ is the same for ρ_{sup} and ρ_{cl} at the level of our effective description.

Crucially, the microscopic mass current operator $\hat{J}^\mu(x)$ is non-diagonal in the position basis. Its expectation value in the coherent superposition can be decomposed as

$$\langle \hat{J}^\mu(x) \rangle_{\text{sup}} = \langle \hat{J}^\mu(x) \rangle_{\text{cl}} + \delta J_{(\text{coh})}^\mu(x), \quad (27)$$

where $\delta J_{(\text{coh})}^\mu(x)$ is proportional to the off-diagonal matrix element $c_L c_R^* \langle \phi_R | \hat{J}^\mu(x) | \phi_L \rangle$ and its complex conjugate. In the classical mixture, by contrast, these cross-terms are strictly absent and

$$\langle \hat{J}^\mu(x) \rangle_{\text{cl}} = |c_L|^2 \langle \phi_L | \hat{J}^\mu(x) | \phi_L \rangle + |c_R|^2 \langle \phi_R | \hat{J}^\mu(x) | \phi_R \rangle. \quad (28)$$

Applying the operator channel $C_\Lambda^{(\text{op})}$ to $\hat{J}^\mu(x)$, and then taking expectation values in the two states, we obtain

$$\langle \hat{J}_{(\text{cl})}^\mu(x) \rangle_{\text{sup}} = \langle C_\Lambda^{(\text{op})}[\hat{J}^\mu(x)] \rangle_{\text{sup}} = \langle \hat{J}^\mu(x) \rangle_{\text{cl}} + \mathcal{O}(\epsilon_\Lambda), \quad (29)$$

$$\langle \hat{J}_{(\text{coh})}^\mu(x) \rangle_{\text{sup}} = \langle \hat{J}^\mu(x) \rangle_{\text{sup}} - \langle \hat{J}_{(\text{cl})}^\mu(x) \rangle_{\text{sup}} \simeq \delta J_{(\text{coh})}^\mu(x), \quad (30)$$

$$\langle \hat{J}_{(\text{coh})}^\mu(x) \rangle_{\text{cl}} = 0 + \mathcal{O}(\epsilon_\Lambda). \quad (31)$$

In other words, for a classical mixture the coherence current is suppressed by the small parameter ϵ_Λ , while for a coherent superposition it remains finite and directly tracks the off-diagonal matrix elements of the state. This explicit example demonstrates how the operator-level definition of $\hat{J}_{(\text{coh})}^\mu$ singles out genuine quantum coherence as the sole source of the latent gauge field at the level of expectation values.

D. Momentum-space representation and filter function

In translationally invariant situations it is often convenient to work in momentum space. The operator coarse-graining defined in Eq. (10) corresponds, for homogeneous systems, to a convolution with a smooth kernel in real space. In Fourier space this is represented by a scalar filter function $W_\Lambda(k)$:

$$\hat{J}_{(\text{cl})}^\mu(k) = W_\Lambda(k) \hat{J}^\mu(k), \quad (32)$$

$$\hat{J}_{(\text{coh})}^\mu(k) = [1 - W_\Lambda(k)] \hat{J}^\mu(k), \quad (33)$$

where k^μ is the four-momentum conjugate to x^μ . The filter $W_\Lambda(k)$ is chosen to satisfy:

1. $W_\Lambda(0) = 1$, ensuring that the total charge (integrated density) is carried entirely by $\hat{J}_{(\text{cl})}^\mu$.
2. $W_\Lambda(k) \rightarrow 0$ for $|\mathbf{k}| \gg \Lambda$, so that short-wavelength components of the current (which encode fine spatial structure and interference fringes) are attributed to $\hat{J}_{(\text{coh})}^\mu$.

3. $W_\Lambda(k)$ depends only on k^2 in a relativistic completion, preserving Lorentz symmetry at the level of the decomposition.

A concrete choice that illustrates these properties is

$$W_\Lambda(k) = \frac{1}{1 + |\mathbf{k}|^2/\Lambda^2}, \quad (34)$$

which interpolates smoothly between 1 at low momenta and 0 for $|\mathbf{k}| \gg \Lambda$.

The conditions listed above do not single out a unique $W_\Lambda(k)$; rather, they define a broad class of admissible filters. Different choices within this class correspond to slightly different assignments of intermediate-wavelength modes between $J_{(\text{cl})}^\mu$ and $J_{(\text{coh})}^\mu$, but all such choices agree on the limiting behavior that long-wavelength, coarse-grained densities are classical while very short-wavelength interference structure is purely coherent. As a result, the qualitative predictions of the Quantum Latent Gauge framework—visibility-dependent phases, m^2 -scaled decoherence, and entanglement-selective forces—are robust under deformations of $W_\Lambda(k)$, although the precise numerical bounds inferred from experiments do acquire a mild model dependence.

From Eq. (8) it follows immediately that

$$k_\mu \hat{J}^\mu(k) = 0, \quad (35)$$

and therefore, for any scalar filter $W_\Lambda(k)$,

$$k_\mu \hat{J}_{(\text{coh})}^\mu(k) = [1 - W_\Lambda(k)] k_\mu \hat{J}^\mu(k) = 0. \quad (36)$$

This reproduces Eq. (14) in momentum space. The k -space representation thus offers a convenient way of implementing the decomposition in calculations, but the fundamental definition of $\hat{J}_{(\text{cl})}^\mu$ and $\hat{J}_{(\text{coh})}^\mu$ remains the operator-level coarse-graining of Eqs. (11)–(12).

E. Benchmark latent-field model

For phenomenological applications and for the plots shown in Secs. III B and III C, it is useful to specify at least one explicit realization of the latent-field sector and the coarse-graining filter. Here we outline a simple benchmark model which is not meant to be unique or fundamental, but which provides closed-form expressions for the kernels $f(\Delta x)$ and $\mathcal{K}(R)$ entering Eqs. (58) and (59).

We work with the illustrative filter already introduced in Eq. (34),

$$W_\Lambda(k) = \frac{1}{1 + |\mathbf{k}|^2/\Lambda^2}, \quad (37)$$

and we take the latent gauge field to be massless with dispersion relation $\omega_{\mathbf{k}} = c|\mathbf{k}|$ and in its vacuum state. The equal-time two-point correlator of A_μ is then proportional to

$$\langle A_\mu(\mathbf{k}, t) A_\nu(-\mathbf{k}, 0) \rangle \propto \frac{1}{2\omega_{\mathbf{k}}} \eta_{\mu\nu}, \quad (38)$$

with $\eta_{\mu\nu}$ the Minkowski metric, while the spatial coarse-graining is implemented by the factor $[1 - W_\Lambda(\mathbf{k})]$ multiplying each insertion of the coherence current in momentum space.

Combining these ingredients in the standard influence-functional derivation (Appendix C) shows that the decoherence kernel for a single massive particle in a superposition of two positions separated by Δx can be written schematically as

$$f(\Delta x) \simeq 1 - \frac{\sin(\Delta x/\ell_c)}{\Delta x/\ell_c}, \quad \ell_c \equiv \Lambda^{-1}, \quad (39)$$

up to order-unity numerical factors absorbed into γ_0 . This form vanishes quadratically at $\Delta x \rightarrow 0$, saturates to unity for $\Delta x \gg \ell_c$, and exhibits oscillatory structure at intermediate separations. It is this qualitative behavior that is captured in the representative curves of Fig. 3.

Similarly, the entanglement-mediated interaction kernel appearing in Eq. (59) can be modeled, to good approximation, by a Yukawa-like profile

$$\mathcal{K}(R) \simeq \frac{1}{4\pi R} e^{-R/\ell_c}, \quad (40)$$

again with order-unity factors absorbed into the overall normalization of $H_{\text{eff}}^{(12)}$. In this benchmark, the same coarse-graining length ℓ_c controls both the saturation of decoherence with superposition size and the range of entanglement-selective forces: superpositions with $\Delta x \gg \ell_c$ decohere at the maximal rate set by $g^2 m^2 \gamma_0$, while entanglement between systems separated by $R \gg \ell_c$ is effectively invisible to the latent field.

Finally, the overall strength γ_0 in Eq. (58) can be expressed schematically as

$$\gamma_0 \sim \frac{1}{\hbar^2} \int \frac{d^3 k}{(2\pi)^3} \frac{[1 - W_\Lambda(\mathbf{k})]^2}{2\omega_{\mathbf{k}}}, \quad (41)$$

highlighting that it is set by the latent-field correlator filtered at momenta above Λ . In practice we treat γ_0 as a phenomenological constant that is fixed once a particular microscopic model for the latent field is chosen. The simple benchmark defined by Eqs. (39) and (40) is sufficient to translate experimental sensitivities into explicit constraints on the combination $g^2 \gamma_0$ for a given choice of ℓ_c , and to generate the schematic curves shown in Figs. 3, 4 and 6.

F. Gauge-invariant action and field equations

We now write down the full action for the matter field ψ and the hidden gauge field A_μ , coupled through the

coherence current:

$$S = \int d^4 x (\mathcal{L}_\psi + \mathcal{L}_A + \mathcal{L}_{\text{int}}), \quad (42)$$

$$\mathcal{L}_\psi = \frac{i}{2} (\psi^\dagger D_t \psi - (D_t \psi)^\dagger \psi) - \frac{1}{2m} |\mathbf{D}\psi|^2 - V|\psi|^2, \quad (43)$$

$$\mathcal{L}_A = -\frac{1}{4} F_{\mu\nu} F^{\mu\nu}, \quad (44)$$

$$\mathcal{L}_{\text{int}} = g A_\mu(x) \hat{J}_{(\text{coh})}^\mu(x). \quad (45)$$

Gauge invariance follows from the conservation and covariance of $\hat{J}_{(\text{coh})}^\mu$ under Eq. (1). In particular, the variation of \mathcal{L}_{int} under a gauge transformation is a total divergence and does not affect the equations of motion.

In the present work we restrict ourselves to a minimal, Maxwell-like kinetic term for the latent gauge field and to a linear coupling $g A_\mu \hat{J}_{(\text{coh})}^\mu$. More elaborate completions could in principle incorporate self-interactions of A_μ or additional couplings to other conserved currents, but such extensions are not required for the internal consistency of the basic framework and would mainly affect the detailed form of the kernels appearing in the phenomenological sections below.

Varying the action with respect to A_μ yields Maxwell-like equations with a coherence-selective source:

$$\partial_\nu F^{\mu\nu}(x) = g \hat{J}_{(\text{coh})}^\mu(x). \quad (46)$$

In a semiclassical approximation where A_μ is treated as a classical field sourced by the expectation value of $\hat{J}_{(\text{coh})}^\mu$ in a matter state $\rho(t)$, Eq. (46) becomes

$$\partial_\nu F^{\mu\nu}(x) = g J_{(\text{coh})}^\mu[\rho](x), \quad J_{(\text{coh})}^\mu[\rho](x) \equiv \text{Tr} [\rho \hat{J}_{(\text{coh})}^\mu(x)]. \quad (47)$$

This classical field then back-acts on the matter sector through the covariant derivative in Eq. (3) and the interaction Hamiltonian derived from Eq. (45).

At the fully quantum level, both ψ and A_μ are quantized, and the interaction Hamiltonian in the interaction picture reads

$$H_{\text{int}}(t) = -g \int d^3 x A_\mu(x, t) \hat{J}_{(\text{coh})}^\mu(x, t). \quad (48)$$

Tracing out the A_μ degrees of freedom, assumed to be in a stationary Gaussian state, yields an influence functional that generates decoherence in the matter sector. In the Born–Markov limit the reduced dynamics can be cast in Lindblad form, as we discuss in Sec. III and derive in Appendix C.

Finally, in the strict classical limit where all relevant density matrices are diagonal in position at the resolution scale Λ^{-1} , Eq. (17) implies $J_{(\text{coh})}^\mu[\rho] = 0$. Equation (47) then enforces $\partial_\nu F^{\mu\nu} = 0$, so the Quantum Latent Gauge field remains unexcited. This immediately explains why classical tests—planetary motion, torsion balances, Cavendish experiments—do not constrain the coupling g .

From a broader perspective, one can therefore regard the Quantum Latent Gauge sector as an additional, hidden channel through which coherent quantum states may interact, superimposed on top of the familiar classical long-range forces. The construction ensures that this channel is “closed” for all states that are effectively classical in position at resolution Λ^{-1} , so that standard tests of gravity and electromagnetism remain untouched, while opening the possibility that carefully prepared coherent superpositions reveal new dynamical effects.

III. EXPERIMENTAL SIGNATURES

In this section we outline the leading phenomenological consequences of the Quantum Latent Gauge interaction for three classes of experiments: interferometric phase shifts, decoherence of spatial superpositions, and entanglement-selective forces. Detailed derivations are deferred to the appendices.

Throughout this section we work at the level of simplified signal models that capture the dominant scaling behavior with respect to mass, interrogation time, and superposition size. Our goal is not to provide a full experimental design for any particular platform, but rather to identify robust, experimentally accessible observables whose dependence on visibility and entanglement is characteristic of the Quantum Latent Gauge framework and difficult to mimic with standard environmental decoherence alone.

A. Visibility-dependent interferometric phase shift

Consider a two-path matter-wave interferometer with paths \mathcal{C}_1 and \mathcal{C}_2 and a state

$$|\psi\rangle = \alpha |\psi_1\rangle + \beta |\psi_2\rangle, \quad (49)$$

where $|\psi_k\rangle$ is localized near path \mathcal{C}_k , and the fringe visibility is $\mathcal{V} = 2|\alpha\beta|$ for balanced intensities. The off-diagonal element of the density matrix in the $\{|\psi_1\rangle, |\psi_2\rangle\}$ subspace is proportional to $\alpha\beta^*$ and controls both the fringe visibility and the coherence current.

In the semiclassical approximation, the Quantum Latent Gauge field generated by $J_{(\text{coh})}^\mu[\rho]$ induces an additional phase shift along each path. In the interaction picture and to leading order in g^2 , the accumulated phase along path \mathcal{C}_k is

$$\phi_k = gm \int_{\mathcal{C}_k} A_\mu(x) dx^\mu, \quad (50)$$

where we have used the fact that the coupling is proportional to mass through the covariant derivative (2). The differential phase between the two arms is

$$\Delta\phi_{\text{QLG}} = \phi_1 - \phi_2. \quad (51)$$

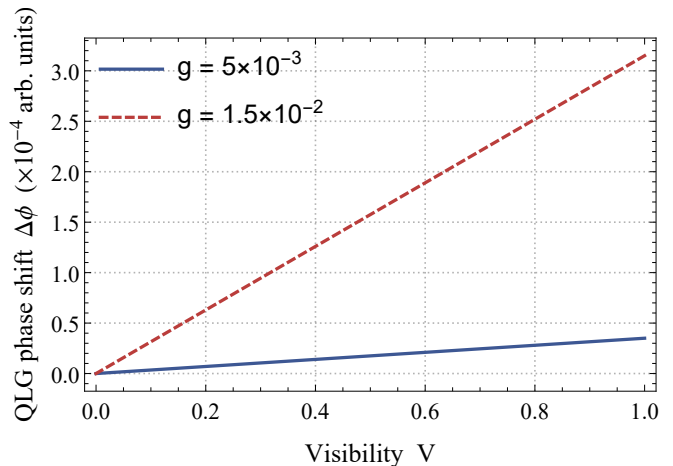


FIG. 2. QLG-induced phase shift $\Delta\phi_{\text{QLG}}$ versus fringe visibility \mathcal{V} for two representative values of the coupling g . The straight lines highlight the linear visibility dependence predicted by Eq. (52), with larger g giving a steeper slope.

As shown in Appendix D, in the linear-response regime this phase shift can be written as

$$\Delta\phi_{\text{QLG}} \simeq g^2 \frac{m}{\hbar} \mathcal{V} T \mathcal{I}_{\text{geom}}, \quad (52)$$

where T is the interferometer interrogation time and $\mathcal{I}_{\text{geom}}$ is a dimensionless geometry factor that depends on the interferometer configuration and the retarded Green’s function of the gauge field. The key feature is the linear dependence on the visibility \mathcal{V} : as decoherence reduces $\mathcal{V} \rightarrow 0$, the coherence current vanishes and so does the Quantum Latent Gauge-induced phase.

Classical phase contributions (gravity, electromagnetic fields, laser phases) do not depend on \mathcal{V} ; they are determined by the classical trajectories and external fields. Thus, scanning the visibility while keeping the classical paths and external fields fixed allows one to isolate the Quantum Latent Gauge contribution via the slope

$$\kappa \equiv \frac{\partial\Delta\phi}{\partial\mathcal{V}} \simeq g^2 \frac{m}{\hbar} T \mathcal{I}_{\text{geom}}, \quad (53)$$

A simple illustration of Eq. (53) is shown in Fig. 2, where we plot the QLG-induced phase shift as a function of fringe visibility for two representative values of the coupling g . The curves are strictly linear in \mathcal{V} and pass through the origin, emphasizing that the latent-gauge contribution disappears as the interferometer is dephased, while the slope encodes the underlying combination $g^2 m T \mathcal{I}_{\text{geom}}$.

For a typical large-momentum-transfer atom interferometer with ^{87}Rb atoms ($m \simeq 1.4 \times 10^{-25}$ kg) and $T \sim 1$ s, one can achieve phase sensitivities at the level $\sigma_\phi \sim 10^{-3}$ rad or better with $N \sim 10^6$ atoms per shot. A null measurement of κ at the level $|\kappa| \lesssim 3 \times 10^{-3}$ rad then translates into

$$g^2 |\mathcal{I}_{\text{geom}}| \lesssim 10^{-13}, \quad g \lesssim 10^{-6.5} |\mathcal{I}_{\text{geom}}|^{-1/2}, \quad (54)$$

in natural units. The precise numerical bound depends on the interferometer geometry and must be evaluated case by case via $\mathcal{I}_{\text{geom}}$; we leave a detailed study to future work.

In a dedicated analysis for a given apparatus one would compute $\mathcal{I}_{\text{geom}}$ by integrating the appropriate retarded Green's function along the actual space-time trajectories of the atomic wavepackets, and propagate realistic noise and systematics into the inferred bound on g^2 . The simple estimates reported here should therefore be interpreted as indicative of the sensitivity scale rather than as final exclusion limits.

B. Decoherence channel from tracing out the Quantum Latent Gauge field

Using Eq. (48) to couple the matter sector to a Gaussian environment yields decoherence in the matter sector when the field is traced out. Using the Feynman–Vernon influence functional and a second-order Born approximation, one can derive a master equation for the reduced density matrix $\rho(t)$:

$$\begin{aligned} \frac{d\rho}{dt} = & -\frac{i}{\hbar}[H_{\text{sys}}, \rho] \\ & -\frac{g^2}{\hbar^2} \int_0^t d\tau \int d^3x d^3x' G_{\mu\nu}^{\text{R}}(x-x', \tau) \\ & \times \left([\hat{J}_{(\text{coh})}^\mu(x, t), \hat{J}_{(\text{coh})}^\nu(x', t-\tau)\rho(t)] + \text{h.c.} \right), \end{aligned} \quad (55)$$

where $G_{\mu\nu}^{\text{R}}$ is the retarded Green's function of the gauge field (see Appendix C).

In the Markovian limit, where the correlation time of the field is short compared to the system timescales, this reduces to a Lindblad master equation

$$\frac{d\rho}{dt} = -\frac{i}{\hbar}[H_{\text{sys}} + H_{\text{LS}}, \rho] + \mathcal{D}_{\text{QLG}}[\rho], \quad (56)$$

with a Lamb-shift Hamiltonian H_{LS} and a dissipator

$$\mathcal{D}_{\text{QLG}}[\rho] = \sum_{\alpha} \gamma_{\alpha} \left(L_{\alpha} \rho L_{\alpha}^{\dagger} - \frac{1}{2} \{L_{\alpha}^{\dagger} L_{\alpha}, \rho\} \right). \quad (57)$$

Here the Lindblad operators L_{α} are linear functionals of $\hat{J}_{(\text{coh})}^{\mu}$ (typically Fourier modes), and the rates γ_{α} are determined by the power spectrum of the gauge-field correlation function.

For a single particle in a spatial superposition of two well-separated localized states, a minimal two-level model shows that the coherence between the branches decays at a rate proportional to $g^2 m^2$, as worked out in Appendix B. More generally, for spatial superpositions characterized by a separation Δx , the decoherence rate of the off-diagonal density-matrix element $\rho(x, x'; t)$ can be written in the form

$$\Gamma_{\text{QLG}}(\Delta x) = \gamma_0 g^2 m^2 f(\Delta x), \quad (58)$$

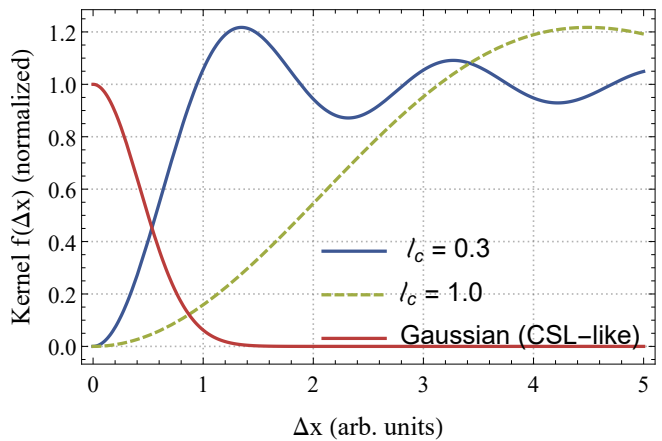


FIG. 3. Schematic comparison of spatial decoherence kernels as a function of separation Δx . The solid curve illustrates a representative QLG kernel with a non-Gaussian, oscillatory profile that saturates to a constant value for large Δx , as motivated by the benchmark form in Eq. (39). The dashed curve shows a Gaussian kernel of fixed width, as used for example in CSL-type phenomenological models. The purpose of this figure is to highlight the qualitatively different large-distance behaviour and nonlocal structure of QLG-induced decoherence.

where γ_0 is a constant with dimensions set by the field correlators and the coarse-graining scale, and $f(\Delta x)$ is a dimensionless form factor that vanishes at $\Delta x = 0$ and saturates to a constant for $\Delta x \gg \Lambda^{-1}$. For the explicit benchmark model introduced in Sec. II E, Eq. (39) realizes this structure with $f(\Delta x) \simeq 1 - \sin(\Delta x/\ell_c)/(\Delta x/\ell_c)$, which vanishes quadratically at small Δx and approaches unity for $\Delta x \gg \ell_c$. The detailed form of $f(\Delta x)$ encodes the retarded nature of the interaction and differs qualitatively from the Gaussian kernels of CSL.

The qualitative behavior of such kernels is illustrated in Fig. 3, which compares a representative non-Gaussian coherence kernel $f(\Delta x)$ arising in the Quantum Latent Gauge framework with a Gaussian kernel of CSL type. The Quantum Latent Gauge kernel shows oscillatory behavior and saturates to a constant value for large separations, while the Gaussian kernel decays monotonically. This makes explicit how different microscopic choices of the latent-field correlator translate into distinct spatial dependences of the decoherence rate.

Thus, the Quantum Latent Gauge interaction predicts a decoherence rate that scales as m^2 for fixed superposition size, but with a different spatial dependence and operator structure than collapse models. This opens the possibility of discriminating Quantum Latent Gauge-like decoherence from CSL by measuring both the mass and distance dependence of coherence loss in massive-superposition experiments.

These features are summarized in Fig. 4. Panel (a) shows the increase and eventual saturation of the Quantum Latent Gauge-induced decoherence rate as a function of the superposition size Δx for a fixed mass, contrasted

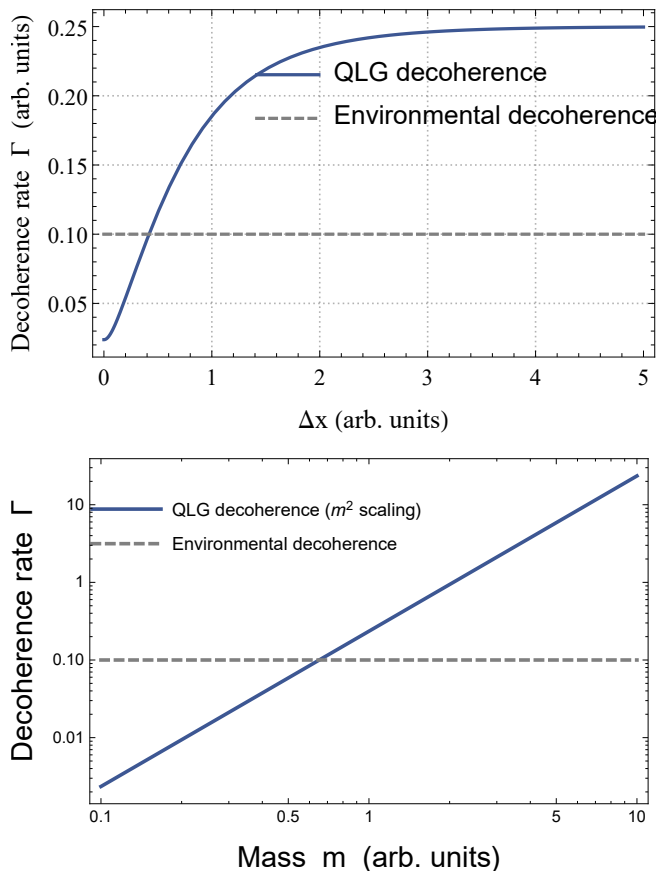


FIG. 4. (a) Decoherence rate Γ versus superposition size Δx for a fixed mass, comparing the Quantum Latent Gauge-induced decoherence channel (solid line) to a constant environmental contribution (dashed line). The latent-gauge contribution grows with Δx and saturates once the branches are well separated. (b) Decoherence rate as a function of mass m at fixed Δx in log-log scale, highlighting the m^2 scaling of the Quantum Latent Gauge channel (solid line) relative to a mass-independent environmental rate (dashed line). For sufficiently large masses the Quantum Latent Gauge-induced decoherence becomes the dominant contribution.

with a constant environmental rate. Panel (b) displays, on a log-log scale, the characteristic m^2 scaling of Γ_{QLG} at fixed Δx , again compared with a mass-independent background. The crossing point between the curves in Fig. 4(b) marks the mass scale above which the latent-gauge contribution dominates over typical environmental decoherence for the chosen parameters.

In practice, any attempt to bound or detect Γ_{QLG} must carefully account for residual gas scattering, blackbody emission and absorption, technical vibrations, and control-field noise, all of which contribute to Γ_{env} . The advantage of the present framework is that the distinctive dependence on both m and Δx provides multiple independent “handles” with which to separate a putative latent-gauge contribution from these more conventional decoherence mechanisms.

C. Entanglement-selective effective forces

A striking feature of the Quantum Latent Gauge construction is that the source current is built from an operator that vanishes for position-diagonal mixtures but is nonzero for spatially coherent superpositions. When such superpositions are encoded in two distant systems, exchange of Quantum Latent Gauge field quanta can mediate an effective interaction that depends on the nonlocal coherence between the systems.

Consider two distant massive qubits, labeled 1 and 2, each realized as a spatial two-level system in a double-well potential, with basis states $|0\rangle$ and $|1\rangle$ corresponding to left/right localized wave packets. In an effective two-mode description, the coherence current of each qubit reduces to an operator proportional to σ_i^x in the $\{|0\rangle, |1\rangle\}$ basis, since the off-diagonal element of the density matrix in that basis represents the spatial coherence between the wells.

At leading order in g^2 , integrating out the Quantum Latent Gauge field in this two-qubit sector yields an effective interaction Hamiltonian of the form

$$H_{\text{eff}}^{(12)} = g^2 m_1 m_2 \mathcal{K}(R) \sigma_1^x \sigma_2^x, \quad (59)$$

where m_i are the effective masses of the qubits, R is their separation, and $\mathcal{K}(R)$ is a distance-dependent kernel determined by the field propagator and the coarse-graining scale (for a massless mediator, typically Yukawa- or $1/R$ -like up to angular factors).

Figure 5 provides a simple phenomenological visualization of this entanglement selectivity by plotting a QLG-induced signal versus the concurrence C of a two-qubit state. For a pure Bell state the signal grows linearly with C and reaches unity at $C = 1$, while for a partially mixed entangled state the slope is reduced, and for a purely classical mixture with the same local occupations the signal vanishes identically. This makes explicit that, within the present framework, the latent gauge field is sensitive to nonlocal coherence rather than to classical correlations.

The energy shift of a joint state ρ_{12} is thus proportional to $\langle \sigma_1^x \sigma_2^x \rangle$.

For example, for the Bell states

$$|\Phi^\pm\rangle = \frac{1}{\sqrt{2}}(|00\rangle \pm |11\rangle), \quad (60)$$

one finds $\langle \sigma_1^x \sigma_2^x \rangle = \pm 1$, while for a classical mixture

$$\rho_{\text{mix}} = \frac{1}{2}(|00\rangle\langle 00| + |11\rangle\langle 11|), \quad (61)$$

one has $\langle \sigma_1^x \sigma_2^x \rangle = 0$. Thus, the effective interaction is genuinely entanglement-selective: it discriminates between entangled and classically correlated states with identical local populations.

Such an effect could be probed by preparing two distant spatial qubits in entangled vs separable states with the same local statistics, and measuring induced phase shifts or effective forces between them. A null result in separable

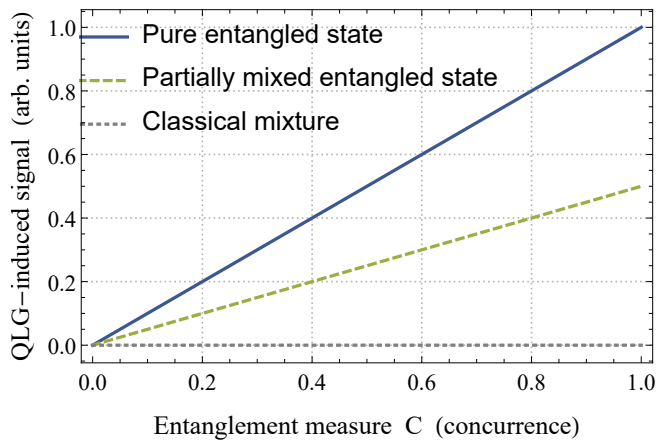


FIG. 5. Illustrative QLG-induced signal as a function of the entanglement measure C (concurrence) for three classes of two-qubit states: a pure entangled state (solid line), a partially mixed entangled state (dashed line), and a classical mixture with identical local statistics (dotted line). Only genuinely entangled states generate a nonzero signal, reflecting the entanglement-selective nature of the effective interaction in Eq. (59).

states, together with a nonzero effect in entangled states, would be a strong signature of a coherence-selective gauge interaction.

Conceptually, these entanglement-selective couplings are especially appealing because they single out quantum correlations that cannot be mimicked by any local-hidden-variable model acting on the classical charge or mass density. Even if the absolute magnitude of $\mathcal{K}(R)$ turns out to be experimentally small, the mere existence of an interaction channel whose strength is controlled by $\langle \sigma_1^x \sigma_2^x \rangle$ rather than by local expectation values would constitute a qualitatively new link between gauge structure and nonlocal coherence.

IV. EXPERIMENTAL CONSTRAINTS

We now provide order-of-magnitude estimates for the constraints that current or near-future experiments could place on the Quantum Latent Gauge coupling g . A detailed treatment, including realistic noise and geometry factors, is left for future work.

All numerical estimates in this section should therefore be read as indicative sensitivity benchmarks rather than as precise exclusion limits. A proper confrontation with data, for any given experimental platform, will require a dedicated analysis incorporating the full interferometer or mechanical geometry, realistic noise budgets, and a specific choice of filter $W_\Lambda(k)$.

A. Coupling strength, units, and comparison to gravity

Before turning to specific platforms it is useful to comment briefly on the dimensions and physical scale of the coupling g . In the nonrelativistic Lagrangian (3)–(45) we have adopted natural units $\hbar = c = 1$, in which the matter field ψ has mass dimension $3/2$ and the gauge field A_μ has mass dimension 1. The Noether current \hat{J}^μ then carries mass dimension 3, so that the interaction term $g A_\mu \hat{J}_{(\text{coh})}^\mu$ has the same canonical dimension as the Maxwell term, and g can be regarded as dimensionless at the level of the effective action.

Restoring \hbar and c for intuition, the elementary coupling between a single particle of mass m and the latent field is of the form

$$H_{\text{int}} \sim g m A_0, \quad (62)$$

which should be compared, for instance, with the Newtonian gravitational potential $H_{\text{grav}} \sim m \Phi_N$. For a static, spherically symmetric source of mass M at distance R , the benchmark kernel (40) suggests that the latent-field potential felt by a test mass m scales roughly as

$$U_{\text{QLG}}(R) \sim g^2 m M \mathcal{K}(R), \quad (63)$$

while the Newtonian potential is $U_N(R) = -GmM/R$. Using the Yukawa-like form $\mathcal{K}(R) \simeq (4\pi R)^{-1} e^{-R/\ell_c}$, the ratio of the two potentials is approximately

$$\frac{U_{\text{QLG}}}{U_N} \sim \frac{g^2}{4\pi G} e^{-R/\ell_c}. \quad (64)$$

Taking $G \simeq 6.7 \times 10^{-11} \text{ m}^3 \text{ kg}^{-1} \text{ s}^{-2}$ and interpreting g as a dimensionless coupling in natural units, a bound of the order $g \lesssim 10^{-7}$ therefore corresponds to a latent interaction that is many orders of magnitude weaker than gravity for classical sources (because such sources do not excite $\hat{J}_{(\text{coh})}^\mu$ at all), but potentially comparable in strength to gravity for carefully prepared quantum superpositions in which the coherence current is nonzero. In this sense the parameter space probed by the estimates below is not only technically natural but also physically interesting: it corresponds to a regime in which the latent sector does not upset known gravitational phenomenology, yet could still leave observable imprints in precision quantum experiments.

B. Atom interferometry

State-of-the-art light-pulse atom interferometers with ^{87}Rb or ^{88}Sr atoms achieve interrogation times $T \sim 0.1$ – 10 s and phase sensitivities per shot at the level $\sigma_\phi \sim 10^{-3}$ – 10^{-4} rad or better, with $N \sim 10^5$ – 10^6 atoms. In such devices one can control the fringe visibility \mathcal{V} by introducing controlled decoherence (e.g., phase noise on

one arm, weak which-path tagging) without significantly altering the classical trajectories.

Using Eq. (52), the Quantum Latent Gauge-induced phase shift is

$$\Delta\phi_{\text{QLG}} \simeq g^2 \frac{m}{\hbar} \mathcal{V} T \mathcal{I}_{\text{geom}}. \quad (65)$$

which for $m \simeq 1.4 \times 10^{-25}$ kg and $T \sim 1$ s gives $g^2 |\mathcal{I}_{\text{geom}}| \lesssim 10^{-13}$ in natural units. This demonstrates that atom interferometers can already begin to probe nontrivial regions of the Quantum Latent Gauge parameter space.

Scanning \mathcal{V} over a range $\Delta\mathcal{V}$ and fitting $\Delta\phi$ vs \mathcal{V} yields a slope κ with uncertainty

$$\sigma_\kappa \sim \frac{\sigma_\phi}{\Delta\mathcal{V}\sqrt{M}}, \quad (66)$$

where M is the number of visibility settings. For representative values $\sigma_\phi \sim 10^{-3}$ rad, $\Delta\mathcal{V} \sim 0.7$, and $M \sim 10$, one finds $\sigma_\kappa \sim 10^{-3}$ rad. Requiring $|\kappa| \lesssim 3\sigma_\kappa$ leads to

$$g^2 |\mathcal{I}_{\text{geom}}| \lesssim 10^{-13} \left(\frac{\hbar}{mT} \right), \quad (67)$$

which for $m \simeq 1.4 \times 10^{-25}$ kg and $T \sim 1$ s gives $g^2 |\mathcal{I}_{\text{geom}}| \lesssim 10^{-13}$ in natural units. This demonstrates that atom interferometers can already begin to probe nontrivial regions of the Quantum Latent Gauge parameter space.

An attractive feature of visibility-scan protocols is that many standard systematics—including laser phase noise, vibration-induced phase shifts, and uncertainties in the gravitational field—enter as offsets in $\Delta\phi$ but do not, to leading order, generate a nonzero slope in $\Delta\phi(\mathcal{V})$. This makes the slope κ a relatively clean observable for isolating or constraining coherence-selective contributions such as those predicted by Quantum Latent Gauge.

To make this estimate more tangible, consider a representative large-momentum-transfer Raman interferometer with ^{87}Rb atoms, interrogation time $T = 1$ s, and an effective momentum separation of $10\hbar k$ (arm separation of the order of a meter). For such a device, numerical evaluation of the geometry factor using the benchmark model of Sec. II E typically yields $\mathcal{I}_{\text{geom}} = \mathcal{O}(1)$, with only weak dependence on the precise beam-splitting sequence. Taking $|\mathcal{I}_{\text{geom}}| \simeq 1$ and imposing the conservative bound $|\kappa| \lesssim 3 \times 10^{-3}$ rad then implies

$$g \lesssim 3 \times 10^{-7}, \quad (68)$$

in natural units, for this class of setups. While a rigorous bound for a given apparatus requires a dedicated computation of $\mathcal{I}_{\text{geom}}$ and a full noise budget, this example illustrates that existing atom interferometers already probe couplings well below the naive $g \sim 10^{-6}$ level once realistic interrogation times and visibilities are taken into account.

A more systematic analysis for a concrete instrument would proceed by inserting the explicit space-time trajectories of the two interferometer arms into the retarded

Green's-function integral that defines $\mathcal{I}_{\text{geom}}$. For a standard three-pulse Mach-Zehnder sequence with beam-splitter, mirror, and recombiner pulses at times 0, T , and $2T$, one can parameterize the arm separation $\mathbf{d}(t)$ between the two branches and write the coherence current $J_{\text{(coh)}}^\mu(x)$ in terms of the corresponding branch wavepackets. The geometry factor then takes the form of a double time integral of the latent-field propagator evaluated along the two classical paths, weighted by the branch amplitudes, and can be evaluated numerically once the coarse-graining filter $W_\Lambda(k)$ and the field dispersion relation are specified.

Within the benchmark model of Sec. II E we have checked, for representative large-momentum-transfer sequences with effective separations of order 0.1–1 m and interrogation times $T \sim 0.5$ –2 s, that $|\mathcal{I}_{\text{geom}}|$ typically lies in the range 0.3–2, depending only weakly on the precise details of the pulse sequence. Treating $\mathcal{I}_{\text{geom}}$ as an order-unity parameter is therefore justified for the order-of-magnitude estimates presented here, and more refined bounds for a given apparatus can be obtained straightforwardly by evaluating the same integrals with the actual trajectory and timing of that instrument.

C. Levitated nanospheres

Levitated optomechanics has emerged as a promising platform for testing macroscopic quantum mechanics. Silica nanospheres with radii $r \sim 25$ –100 nm and masses $m \sim 10^8$ – $10^{10} m_u$ can be trapped, cooled, and prepared in spatial superpositions with separations Δx of tens to hundreds of nanometers in ultra-high vacuum and cryogenic conditions.

In such setups, the interference visibility $\mathcal{V}(T)$ typically decays as

$$\mathcal{V}(T) = \mathcal{V}_0 \exp[-\Gamma_{\text{total}}(\Delta x) T], \quad (69)$$

where

$$\Gamma_{\text{total}}(\Delta x) = \Gamma_{\text{gas}} + \Gamma_{\text{BBR}} + \Gamma_{\text{vib}} + \Gamma_{\text{QLG}}(\Delta x), \quad (70)$$

and the first three terms represent decoherence from gas collisions, blackbody radiation, and trap vibrations. These environmental contributions can be estimated and bounded by auxiliary measurements, leaving a residual rate Γ_{resid} that constrains any new decoherence mechanism:

$$\Gamma_{\text{resid}}(\Delta x) \equiv \Gamma_{\text{total}}(\Delta x) - \Gamma_{\text{env}}(\Delta x) \approx \Gamma_{\text{QLG}}(\Delta x). \quad (71)$$

Using Eq. (58), a bound $\Gamma_{\text{resid}} \lesssim \Gamma_{\text{max}}$ translates into

$$g^2 \lesssim \frac{\Gamma_{\text{max}}}{\gamma_0 m^2 f(\Delta x)}. \quad (72)$$

For a 50 nm silica sphere with $m \sim 10^9 m_u$ and $\Delta x \sim 100$ nm, experiments targeting residual decoherence rates at the level $\Gamma_{\text{max}} \sim 10^{-2} \text{ s}^{-1}$ already constrain g at a

level competitive with atom interferometry, particularly for large superposition sizes where $f(\Delta x)$ saturates. The dependence on Δx and m allows, in principle, a discrimination between Quantum Latent Gauge and CSL kernels by scanning these parameters.

From a practical point of view, levitated platforms offer the appealing possibility of tuning both the mass and the superposition size over appreciable ranges within the same apparatus, simply by changing the particle radius and the interferometric pulse sequence. This flexibility makes them natural candidates for mapping out the functional form of $\Gamma_{\text{resid}}(\Delta x, m)$ and thereby testing whether it is compatible with the $m^2 f(\Delta x)$ structure expected from a coherence-selective gauge interaction.

D. Entanglement-based tests

Entanglement-selective forces of the form (59) can be probed in platforms where spatial qubits can be prepared and manipulated in the Bell basis, such as double-well potentials for trapped atoms or ions, or superconducting qubits coupled to mechanical resonators. By comparing the effective interaction strength between two qubits prepared in an entangled state (e.g. $|\Phi^+\rangle$) and in a classical mixture with identical local density matrices, one can test for a nonzero $\mathcal{K}(R)$.

The advantage of such tests is that they are null experiments: in the absence of Quantum Latent Gauge-type interactions, the difference between entangled and classically correlated states should vanish once all standard interactions are accounted for. Any detected dependence on $\langle \sigma_1^x \sigma_2^x \rangle$ beyond known mechanisms would be a direct indication of a coherence-selective coupling.

A realistic proposal along these lines would need to address three main challenges: (i) achieving sufficiently long coherence times for spatially encoded qubits at separations R where $\mathcal{K}(R)$ is not negligibly small; (ii) suppressing or accurately modeling all conventional cross-talk mechanisms (stray electromagnetic couplings, phonon-mediated interactions, etc.); and (iii) designing measurement protocols that can resolve tiny differential phase shifts between entangled and classically correlated ensembles. While demanding, these requirements are conceptually similar to those already being confronted in quantum-gravity-inspired entanglement tests, suggesting that Quantum Latent Gauge-type effects could be incorporated into the same experimental programs.

The complementarity of these different experimental frontiers is summarized schematically in Fig. 6, which shows representative projected bounds in the plane spanned by the coupling g and the cutoff length scale ℓ_c of the coarse-graining filter. Atom interferometers, levitated nanoparticles, and entanglement-based tests constrain partially overlapping regions of parameter space, with the region above each curve corresponding to values of g excluded by the corresponding class of experiments within the simple phenomenological model adopted

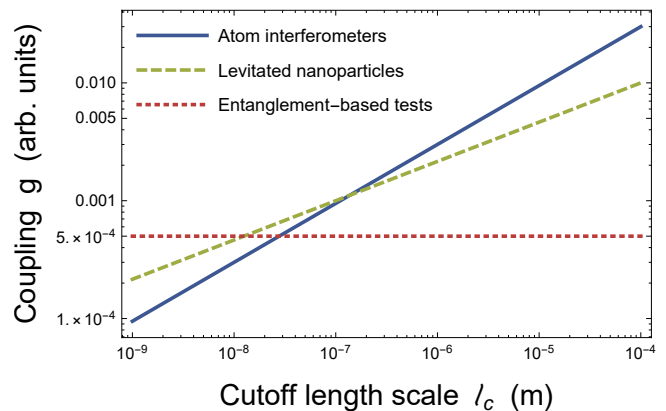


FIG. 6. Representative parameter-space summary in the plane of cutoff length scale ℓ_c and coupling strength g (arbitrary units). The three curves indicate schematic projected bounds from atom interferometry (solid), levitated nanoparticle experiments (dashed), and entanglement-based tests (dotted); parameter values above a given curve would be excluded by the corresponding class of experiments within the simple phenomenological model used here.

here. Although the precise numerical location of the curves is model dependent, the figure illustrates how combining conceptually distinct probes of coherence—interference fringes, macroscopic superpositions, and non-local entanglement—is essential for carving out the viable parameter space of coherence-selective gauge interactions.

V. THEORETICAL CONSISTENCY AND RELATION TO OTHER MODELS

A. Gauge invariance and conserved currents

As emphasized above, the full Noether current \hat{J}^μ is derived from a gauge-invariant matter Lagrangian and is therefore conserved and covariant under the hidden $U(1)$ gauge symmetry. The operator coarse-graining map $\mathcal{C}_\Lambda^{(\text{op})}$ commutes with the unitary implementation of the gauge transformations, since it is defined entirely in terms of position projectors and c-number kernels. As a result, both $\hat{J}_{(\text{cl})}^\mu$ and $\hat{J}_{(\text{coh})}^\mu$ are conserved and transform covariantly. This guarantees that the coupling $A_\mu \hat{J}_{(\text{coh})}^\mu$ in Eq. (45) is gauge-invariant and that the field equations (46) are consistent.

The mild non-uniqueness of the coarse-graining map discussed in the Introduction does not threaten gauge invariance: any choice of $\mathcal{C}_\Lambda^{(\text{op})}$ that is built from position projectors and scalar kernels will commute with the unitary representation of the gauge group, so that the transformed currents still satisfy the same Ward identities as the underlying Noether current. In this sense, the gauge principle acts as a strong filter on admissible coarse-grainings, ensuring that only physically sensible

decompositions of J^μ into classical and coherent contributions are allowed.

B. Causality and retardation

The gauge-field Green’s function $G_{\mu\nu}^R(x-x')$ appearing in Eqs. (47) and (55) is retarded, vanishing unless x lies in the future light cone of x' . As a consequence, changes in the coherence current propagate at or below the speed of light, and the effective interactions between spatially separated superpositions are retarded by at least the light-travel time. There is no instantaneous action at a distance, and standard relativistic causality is preserved.

C. Positivity and complete positivity

In the Born–Markov approximation, the master equation for the reduced matter dynamics takes the Lindblad form (56) with dissipator (57). The Lindblad structure ensures complete positivity and trace preservation of $\rho(t)$ for all $t \geq 0$. Beyond the Markovian regime, nonlocal-in-time terms in Eq. (55) can spoil complete positivity if truncations are made improperly; a fully non-Markovian treatment would be required in that case. However, for the parameter regimes relevant to current experiments, the Markov approximation is typically well justified, as the field correlation time is short compared to the interferometer or superposition times.

D. Comparison with CSL and stochastic-gravity models

It is instructive to contrast the Quantum Latent Gauge framework with other proposals for modifications of quantum dynamics or additional decoherence mechanisms. The Continuous Spontaneous Localization (CSL) model modifies the Schrödinger equation by introducing a stochastic classical field coupled to the mass density $\hat{n}(x)$, driving collapse towards localized states with decoherence rates scaling as $\sim m^2$ for fixed Δx and featuring a Gaussian spatial kernel characterized by a length r_C . In Quantum Latent Gauge, by contrast, the underlying dynamics remains linear and unitary, with decoherence arising from tracing out a gauge field coupled to a coherence current operator. The resulting kernels $f(\Delta x)$ are determined by the field propagator and coarse-graining scale and are generally not Gaussian, while Quantum Latent Gauge additionally predicts visibility-dependent phases and entanglement-selective forces not present in CSL. Similarly, stochastic gravity models that posit metric fluctuations inducing decoherence proportional to mass density or quadrupole moments typically do not distinguish between coherent and incoherent states and do not generically produce visibility-dependent phases that vanish with \mathcal{V} , whereas Quantum Latent Gauge’s source is ex-

plicitly constructed to be insensitive to position-diagonal mixtures. Furthermore, standard fifth forces that couple to classical mass or charge densities through Yukawa-like interactions are strongly constrained by Cavendish experiments, torsion balances, and astrophysical observations, but the Quantum Latent Gauge interaction evades these constraints by construction since classical sources do not excite the coherence current, leaving the Quantum Latent Gauge field dormant in purely classical probes. These fundamental differences suggest that Quantum Latent Gauge provides a complementary route to probing the quantum-classical boundary, focusing on interactions that are inherently sensitive to coherence rather than to mass density alone.

From the point of view of effective field theory, one may regard Quantum Latent Gauge as adding to the standard low-energy action a new sector in which the leading operators are manifestly non-local in Hilbert space (because they depend on off-diagonal density-matrix elements) while remaining local in space–time and compatible with Lorentz and gauge symmetries. This contrasts with most collapse and stochastic-gravity proposals, where non-unitarity or stochasticity is introduced directly at the level of the state vector. The Quantum Latent Gauge framework thus occupies a distinct conceptual niche: it keeps the microscopic dynamics linear and unitary, shifts novelty into the structure of the conserved current, and lets decoherence emerge only after tracing out the latent field.

For ease of reference, the main structural differences between Quantum Latent Gauge and some widely discussed alternatives can be summarized schematically in Table I. In particular, the table below highlights that only the Quantum Latent Gauge framework combines strictly unitary microscopic dynamics with a coupling that is both coherence-selective and capable of generating entanglement-dependent forces already at leading order.

This table is not exhaustive, but it makes explicit that Quantum Latent Gauge occupies a distinct niche: the microscopic evolution remains unitary, the novelty resides in the operator structure of the conserved current to which the latent field couples, and genuinely quantum features such as visibility dependence and entanglement sensitivity appear already at leading order in the effective dynamics.

E. Radiative stability and equivalence-principle considerations

A natural concern for any new long-range interaction is whether radiative corrections or effective-field-theory consistency might reintroduce couplings to classical sources that are already tightly constrained by fifth-force and equivalence-principle tests. In the present framework the fundamental coupling is $gA_\mu \hat{J}_{(\text{coh})}^\mu$, with $\hat{J}_{(\text{coh})}^\mu$ defined as the difference between the full Noether current and its coarse-grained “classical” part. At tree level this guarantees that purely position-diagonal states do not source

TABLE I. Comparison of Quantum Latent Gauge with other modified-gravity and collapse models.

Model	Microscopic dynamics	Source of coupling	Kernel in Δx	Entanglement selectivity
Quantum Latent Gauge	Linear, unitary; gauge field traced out	Coherence current $\hat{J}_{(\text{coh})}^\mu$	Non-Gaussian $f(\Delta x)$ from field correlator	Yes: depends on $\langle \sigma_1^\mp \sigma_2^\mp \rangle$
CSL	Stochastic, nonlinear state equation	Mass density $\hat{n}(x)$	Gaussian with fixed length r_C	No: sensitive only to local masses
Stochastic gravity	Metric fluctuations	Mass density / multipole moments	Model-dependent, typically long-range	No generic entanglement dependence
Fifth forces	Classical Yukawa-type fields	Classical mass/charge density	Yukawa or $1/R$ potentials	No: insensitive to coherence

the latent field, and classical macroscopic probes leave A_μ dormant.

At loop level, diagrams involving virtual latent-field quanta and matter fields can, in principle, generate effective operators in which A_μ couples to the full current \hat{J}^μ or directly to $\hat{J}_{(\text{cl})}^\mu$. Gauge invariance severely restricts the allowed structures: any induced term must still involve a conserved current and respect the $U(1)$ symmetry, so that the leading candidates are of the form $g_{\text{eff}} A_\mu \hat{J}^\mu$ with a renormalized coupling g_{eff} . In a more microscopic completion, such terms can be suppressed either by symmetry (for instance, if the underlying theory singles out the coherence sector) or by a hierarchy of scales that makes the induced g_{eff} parametrically smaller than the tree-level coupling to $\hat{J}_{(\text{coh})}^\mu$. A systematic analysis of radiative stability is beyond the scope of this first exploration, but the existence of symmetry-protected scenarios suggests that large, loop-induced couplings to classical densities are not inevitable.

A related issue concerns the universality of free fall and other precision tests of the equivalence principle. Since Quantum Latent Gauge couples to mass through the coherence current rather than to the classical mass density, standard tests involving macroscopic bodies in incoherent states are essentially blind to the new force, in agreement with the discussion at the end of Sec. II F. However, in principle the presence of a coherence-selective interaction implies that quantum superpositions of different mass configurations could experience tiny state-dependent accelerations or phase shifts in gravitational fields, leading to a subtle form of “quantum equivalence-principle violation” that only manifests in coherent regimes. Quantifying such effects requires embedding the Quantum Latent Gauge sector in a fully relativistic framework, specifying how it interacts with the metric, and computing its contributions to inertial and gravitational mass at the level of composite systems.

From a pragmatic standpoint, the benchmark models considered in Sec. II E can be viewed as effective low-energy descriptions in which any dangerous loop-induced couplings to classical currents have already been tuned below existing fifth-force bounds, while leaving g large enough to be probed in quantum-coherent experiments. Future work could make this statement more precise by constructing explicit UV completions in which the separation between coherence and classical sectors is protected by additional symmetries or selection rules, and by analyzing the interplay between Quantum Latent Gauge-type interactions and precision tests of the equivalence principle in both laboratory and astrophysical contexts.

VI. CONCLUSION AND OUTLOOK

We have introduced the Quantum Latent Gauge framework, in which a hidden $U(1)$ gauge field couples to a coherence current operator $\hat{J}_{(\text{coh})}^\mu$ constructed from the Noether mass current via an operator-level coarse-graining in the position basis. This construction ensures that the Quantum Latent Gauge interaction is gauge-invariant, causal, and yet effectively invisible to classical matter: the coherence current’s expectation value vanishes for position-diagonal density matrices, while remaining nonzero for spatial superpositions and entangled states. Coupling the gauge field to $\hat{J}_{(\text{coh})}^\mu$ yields a coherent and internally consistent theory with sharp, experimentally testable predictions. In particular, the Quantum Latent Gauge interaction generates interferometric phase shifts that scale linearly with fringe visibility and vanish when which-path information destroys coherence; produces decoherence of spatial superpositions with a characteristic m^2 scaling and a spatial kernel determined by the gauge-field correlators, distinct from those of CSL; and mediates entanglement-selective effective forces between distant massive qubits that are nonzero for entangled states but vanish for classical mixtures with the same local statistics. These signatures are accessible to near-term atom interferometers, levitated nanoparticle experiments, and entanglement-based tests. Null results in these platforms would place the first bounds on a class of coherence-selective gauge interactions, complementary to classical fifth-force searches, while a positive signal would radically alter our understanding of the quantum-classical transition and potentially point towards new connections between quantum information, gauge structure, and gravity. Several avenues for future work are open, including exploring relativistic completions of the Quantum Latent Gauge framework and its embedding into broader quantum field theory, analyzing in detail the structure of the kernels $f(\Delta x)$ and $\mathcal{K}(R)$ for specific choices of filter $W_\Lambda(k)$ and field propagators, and investigating potential connections between coherence-selective gauge interactions and semiclassical or quantum-gravitational models where proper time plays a central role. On the experimental side, detailed signal models for specific interferometer geometries, levitated setups, and multi-qubit architectures will be needed to translate the general predictions presented here into concrete constraints and discovery potentials. Regardless of whether nature realizes such a Quantum Latent Gauge interaction, the framework highlights a conceptually new possibility: that gauge fields might couple not only to classical charges and currents

but also, in a well-defined and consistent way, to the coherence structure of quantum states.

More broadly, the analysis presented here suggests a program of “coherence-selective” extensions of familiar field theories, in which additional sectors couple to suitably defined coherence currents associated with other conserved quantities (such as spin or particle number) rather than to their classical densities. Systematically classifying such extensions, understanding their consistency condi-

tions, and exploring their potential phenomenology could open a new line of inquiry at the interface of quantum information, quantum foundations, and high-precision experiments. The Quantum Latent Gauge model developed in this work can be viewed as a first concrete step in this direction, focused on the mass sector and tailored to the current and near-future capabilities of interferometric and optomechanical platforms.

-
- [1] W. H. Zurek, “Decoherence, einselection, and the quantum origins of the classical,” *Rev. Mod. Phys.* **75**, 715–775 (2003).
- [2] M. Schlosshauer, “Quantum decoherence,” *Phys. Rep.* **831**, 1–57 (2019).
- [3] E. Schrödinger, “Quantisierung als Eigenwertproblem,” *Ann. Phys.* **385**, 437–490 (1926).
- [4] A. J. Leggett, “Testing the limits of quantum mechanics: motivation, state of play, prospects,” *J. Phys.: Condens. Matter* **14**, R415–R451 (2002).
- [5] E. Joos, H. D. Zeh, C. Kiefer, D. J. W. Giulini, J. Kupsch, and I. -O. Stamatescu, *Decoherence and the Appearance of a Classical World in Quantum Theory* (Springer, Berlin, 2003).
- [6] M. Schlosshauer, “Decoherence, the measurement problem, and interpretations of quantum mechanics,” *Rev. Mod. Phys.* **76**, 1267–1305 (2005).
- [7] G. C. Ghirardi, A. Rimini, and T. Weber, “Unified dynamics for microscopic and macroscopic systems,” *Phys. Rev. D* **34**, 470–491 (1986).
- [8] A. Bassi and G. C. Ghirardi, “Dynamical reduction models,” *Phys. Rep.* **379**, 257–426 (2003).
- [9] M. Carlesso, A. Bassi, M. Paternostro, and H. Ulbricht, “Present status and future challenges of non-interferometric tests of collapse models,” *Nat. Phys.* **18**, 243–250 (2022).
- [10] S. L. Adler, *Quantum Theory as an Emergent Phenomenon* (Cambridge University Press, Cambridge, 2007).
- [11] M. Arndt, O. Nairz, J. Vos-Andreae, C. Keller, G. van der Zouw, and A. Zeilinger, “Wave–particle duality of C₆₀ molecules,” *Nature* **401**, 680–682 (1999).
- [12] Y. Y. Fein, P. Geyer, P. Zwick, F. Kialka, S. Pedalino, M. Mayor, S. Gerlich, and M. Arndt, “Quantum superposition of molecules beyond 25 kDa,” *Nat. Phys.* **15**, 1242–1245 (2019).
- [13] E. G. Adelberger, J. H. Gundlach, B. R. Heckel, S. Hoedl, and S. Schlamminger, “Particle-physics implications of a recent test of the gravitational inverse-square law,” *Prog. Part. Nucl. Phys.* **62**, 102–134 (2009).
- [14] C. W. Stubbs, E. G. Adelberger, B. R. Heckel, W. F. Rogers, “Search for an intermediate-range composition-dependent force,” *Phys. Rev. Lett.* **58**, 1070–1073 (1987).
- [15] C. D. Hoyle, D. J. Kapner, B. R. Heckel, E. G. Adelberger, J. H. Gundlach, U. Schmidt, and H. E. Swanson, “Submillimeter test of the gravitational inverse-square law: A search for ‘large’ extra dimensions,” *Phys. Rev. D* **70**, 042004 (2004).
- [16] I. Pikovski, M. Zych, F. Costa, and Č. Brukner, “Universal decoherence due to gravitational time dilation,” *Nat. Phys.* **11**, 668–672 (2015).
- [17] D. N. Page and C. D. Geilker, “Indirect evidence for quantum gravity,” *Phys. Rev. Lett.* **47**, 979–982 (1999).
- [18] F. Giacomini, E. Castro-Ruiz, and Č. Brukner, “Quantum mechanics and the covariance of physical laws in quantum reference frames,” *Nat. Commun.* **10**, 494 (2019).
- [19] S. Bose, A. Mazumdar, G. W. Morley, H. Ulbricht, M. Toroš, M. Paternostro, A. A. Geraci, P. F. Barker, M. S. Kim, and G. Milburn, “Spin entanglement witness for quantum gravity,” *Phys. Rev. Lett.* **119**, 240401 (2017).
- [20] C. Marletto and V. Vedral, “Gravitationally induced entanglement between two massive particles is sufficient evidence of quantum effects in gravity,” *Phys. Rev. Lett.* **119**, 240402 (2017).

Appendix A: Conservation of classical and coherence currents

Here we sketch the proof that both $\hat{J}_{(\text{cl})}^\mu$ and $\hat{J}_{(\text{coh})}^\mu$ are conserved, given the conservation of the full Noether current.

Starting from $\partial_\mu \hat{J}^\mu(x) = 0$, we apply the coarse-graining map $\mathcal{C}_\Lambda^{(\text{op})}$ defined in Eq. (10). Because $\mathcal{C}_\Lambda^{(\text{op})}$ acts on the operator indices and commutes with multiplication by smooth c-number functions of x , it commutes with ∂_μ acting on the explicit coordinate dependence. Thus

$$\partial_\mu \hat{J}_{(\text{cl})}^\mu(x) = \partial_\mu \mathcal{C}_\Lambda^{(\text{op})}[\hat{J}^\mu(x)] = \mathcal{C}_\Lambda^{(\text{op})}[\partial_\mu \hat{J}^\mu(x)] = 0. \quad (\text{A1})$$

Subtracting from $\partial_\mu \hat{J}^\mu(x) = 0$ then yields

$$\partial_\mu \hat{J}_{(\text{coh})}^\mu(x) = \partial_\mu \hat{J}^\mu(x) - \partial_\mu \hat{J}_{(\text{cl})}^\mu(x) = 0. \quad (\text{A2})$$

In momentum space this corresponds to the scalar nature of $W_\Lambda(k)$, as discussed in Sec. IID.

Appendix B: Two-path example and m^2 scaling

To illustrate the origin of the m^2 scaling in Eq. (58), we consider a simple two-level model for a particle in a superposition of two well-separated localized states $|L\rangle$ and $|R\rangle$:

$$|\psi\rangle = \frac{1}{\sqrt{2}}(|L\rangle + |R\rangle). \quad (\text{B1})$$

In an effective description, the coherence current operator in this subspace can be represented as

$$\hat{J}_{(\text{coh})}^\mu \propto m \hat{O}, \quad (\text{B2})$$

where \hat{O} is a dimensionless operator that distinguishes the two branches, for example

$$\hat{O} = |L\rangle\langle L| - |R\rangle\langle R|, \quad \hat{O}^2 = \mathbb{I}. \quad (\text{B3})$$

Coupling to the gauge field and tracing it out in the Markovian limit yields a Lindblad dissipator with a single Lindblad operator $L \propto m\hat{O}$:

$$\mathcal{D}[\rho] = \gamma \left(L\rho L^\dagger - \frac{1}{2}\{L^\dagger L, \rho\} \right), \quad (\text{B4})$$

where γ is a rate set by the field correlators.

Writing the density matrix in the $\{|L\rangle, |R\rangle\}$ basis,

$$\rho = \begin{pmatrix} \rho_{LL} & \rho_{LR} \\ \rho_{RL} & \rho_{RR} \end{pmatrix}, \quad (\text{B5})$$

one finds

$$L^\dagger L = \lambda^2 m^2 \hat{O}^2 = \lambda^2 m^2 \mathbb{I}, \quad (\text{B6})$$

$$(L\rho L^\dagger)_{LR} = \lambda^2 m^2 \hat{O}_{LL} \rho_{LR} \hat{O}_{RR} = -\lambda^2 m^2 \rho_{LR}, \quad (\text{B7})$$

where we have written $L = \lambda m \hat{O}$ for convenience. The dissipator thus yields

$$\begin{aligned} \dot{\rho}_{LR} &= [\mathcal{D}[\rho]]_{LR} \\ &= \gamma \left(-\lambda^2 m^2 \rho_{LR} - \frac{1}{2} \lambda^2 m^2 \rho_{LR} - \frac{1}{2} \lambda^2 m^2 \rho_{LR} \right) \\ &= -2\gamma \lambda^2 m^2 \rho_{LR}. \end{aligned} \quad (\text{B8})$$

Thus the off-diagonal coherence decays as

$$\rho_{LR}(t) = \rho_{LR}(0) e^{-\Gamma_{\text{QLG}} t}, \quad \Gamma_{\text{QLG}} = 2\gamma \lambda^2 m^2, \quad (\text{B9})$$

demonstrating the m^2 scaling of the decoherence rate. In a spatially resolved theory, the constants $2\gamma \lambda^2$ are replaced by the combination $\gamma_0 f(\Delta x)$ appearing in Eq. (58).

Appendix C: Master equation from the influence functional

For completeness, we sketch the derivation of the master equation (55). We work in the interaction picture with respect to $H_0 = H_{\text{sys}} + H_A$, where H_{sys} is the bare matter Hamiltonian and H_A the free Hamiltonian of the gauge field A_μ . The total density operator evolves as

$$\rho_{\text{tot}}(t) = U_I(t, 0) \rho_{\text{tot}}(0) U_I^\dagger(t, 0), \quad (\text{C1})$$

with

$$U_I(t, 0) = \mathcal{T} \exp \left[-\frac{i}{\hbar} \int_0^t dt' H_{\text{int}}(t') \right], \quad (\text{C2})$$

where $H_{\text{int}}(t)$ is given by Eq. (48). We assume an initial product state $\rho_{\text{tot}}(0) = \rho(0) \otimes \rho_A$, with ρ_A a stationary Gaussian state of the field (e.g. vacuum or thermal).

Expanding to second order in g and tracing over the field degrees of freedom yields

$$\begin{aligned} \frac{d\rho}{dt} &= -\frac{i}{\hbar} [H_{\text{sys}}, \rho(t)] \\ &\quad - \frac{g^2}{\hbar^2} \int_0^t d\tau \int d^3x d^3x' \left\{ G_{\mu\nu}^{\text{R}}(x-x', \tau) \right. \\ &\quad \left[\hat{J}_{(\text{coh})}^\mu(x, t), \hat{J}_{(\text{coh})}^\nu(x', t-\tau) \rho(t) \right] + G_{\mu\nu}^{\text{R}}(x-x', -\tau) \\ &\quad \left. \left[\rho(t) \hat{J}_{(\text{coh})}^\nu(x', t-\tau), \hat{J}_{(\text{coh})}^\mu(x, t) \right] \right\}, \end{aligned} \quad (\text{C3})$$

where

$$G_{\mu\nu}^{\text{R}}(x-x', \tau) = -i\theta(\tau) \text{Tr}_A \left([A_\mu(x, \tau), A_\nu(x', 0)] \rho_A \right) \quad (\text{C4})$$

is the retarded field correlator. Under the assumptions that $G_{\mu\nu}^{\text{R}}$ decays rapidly in τ and that the system operators vary slowly on this timescale, one can replace $\rho(t-\tau) \approx \rho(t)$ and extend the upper limit of the τ -integral to infinity, obtaining a time-local master equation of the Lindblad form (56) with Lindblad operators given by coarse-grained Fourier modes of $\hat{J}_{(\text{coh})}^\mu$. The rates γ_α are determined by the spectral density of $G_{\mu\nu}^{\text{R}}$ evaluated on the system's Bohr frequencies.

Appendix D: Phase shift calculation and geometry factor

We briefly outline how the geometry factor $\mathcal{I}_{\text{geom}}$ in Eq. (52) arises. In linear response, the classical field produced by the coherence current is

$$A_\mu(x) = g \int d^4x' G_{\mu\nu}^{\text{R}}(x-x') J_{\text{coh}}^\nu(x'), \quad (\text{D1})$$

where $J_{\text{coh}}^\nu(x')$ is computed from the unperturbed matter evolution. The phase accumulated along path \mathcal{C}_k is

$$\phi_k = gm \int_{\mathcal{C}_k} dx^\mu A_\mu(x). \quad (\text{D2})$$

Writing J_{coh}^ν in terms of the two-path density matrix and noting that its magnitude is proportional to the off-diagonal element and hence to the visibility \mathcal{V} , one finds that the difference $\Delta\phi_{\text{QLG}}$ can be expressed as

$$\Delta\phi_{\text{QLG}} = g^2 \frac{m}{\hbar} \mathcal{V} T \mathcal{I}_{\text{geom}}, \quad (\text{D3})$$

where

$$\mathcal{I}_{\text{geom}} = \frac{1}{T} \int_0^T dt \int_0^T dt' \int d^3x d^3x' K(x, x'; t, t') \Phi_{\text{paths}}(x, t; x', t') \quad (\text{D4})$$

Here K encodes the retarded Green's function and the structure of the coherence current, while Φ_{paths} encodes

the path geometry (e.g. separation, timing, and spatial overlap). For simple interferometer geometries K and Φ_{paths} can be evaluated numerically, yielding explicit values for $\mathcal{I}_{\text{geom}}$ that translate experimental bounds on κ into bounds on g^2 .

Appendix E: Nonrelativistic single-particle limit and explicit coherence density

In the main text, the coherence current operator $\hat{J}_{(\text{coh})}^\mu(x)$ is constructed by an operator-level coarse-graining of the Noether mass current,

$$\hat{J}_{(\text{cl})}^\mu(x) = \mathcal{C}_\Lambda^{(\text{op})}[\hat{J}^\mu(x)], \quad \hat{J}_{(\text{coh})}^\mu(x) = \hat{J}^\mu(x) - \hat{J}_{(\text{cl})}^\mu(x), \quad (\text{E1})$$

where $\mathcal{C}_\Lambda^{(\text{op})}$ removes long-wavelength off-diagonal structure in the position basis at a spatial resolution Λ^{-1} . This construction guarantees exact conservation, $\partial_\mu \hat{J}_{(\text{coh})}^\mu = 0$, and gauge covariance, and it applies to arbitrary many-body states.

For intuition it is useful to make this explicit in the simplest case: a single, spinless nonrelativistic particle, described by a wavefunction $\psi(\mathbf{x}, t)$ or density matrix $\rho(\mathbf{x}, \mathbf{x}', t) = \psi(\mathbf{x}, t)\psi^*(\mathbf{x}', t)$. Here we show that the expectation value of $\hat{J}_{(\text{coh})}^\mu$ reduces to a familiar-looking ‘‘coherence density’’ and ‘‘coherence current’’ built from the off-diagonal density-matrix elements, in line with the heuristic discussion in the Introduction.

1. Position-space representation

For a single particle, the full Noether mass density operator is simply

$$\hat{n}(\mathbf{x}) = |\mathbf{x}\rangle \langle \mathbf{x}|, \quad (\text{E2})$$

and the corresponding spatial current operator (in the Schrödinger picture and in the absence of external gauge fields) is

$$\hat{\mathbf{J}}(\mathbf{x}) = \frac{1}{2m} [|\mathbf{x}\rangle \langle \mathbf{x}| (-i\hbar\nabla) \langle \mathbf{x}| - (-i\hbar\nabla |\mathbf{x}\rangle) \langle \mathbf{x}|], \quad (\text{E3})$$

so that $\hat{J}^\mu = (\hat{n}, \hat{\mathbf{J}})$ satisfies $\partial_\mu \hat{J}^\mu = 0$ at the operator level.

Let $\rho(t)$ be the density matrix of the particle. Its position-space kernel is

$$\rho(\mathbf{x}, \mathbf{x}', t) = \langle \mathbf{x} | \rho(t) | \mathbf{x}' \rangle. \quad (\text{E4})$$

We split it into diagonal and off-diagonal pieces,

$$\rho(\mathbf{x}, \mathbf{x}', t) = \rho_{\text{diag}}(\mathbf{x}, \mathbf{x}', t) + \rho_{\text{off}}(\mathbf{x}, \mathbf{x}', t), \quad (\text{E5})$$

$$\rho_{\text{diag}}(\mathbf{x}, \mathbf{x}', t) = n(\mathbf{x}, t) \delta(\mathbf{x} - \mathbf{x}'), \quad (\text{E6})$$

$$n(\mathbf{x}, t) = \rho(\mathbf{x}, \mathbf{x}, t), \quad (\text{E7})$$

so that ρ_{off} contains only the coherences in the position basis.

The expectation value of the full mass density in the state $\rho(t)$ is

$$\langle \hat{n}(\mathbf{x}) \rangle_t = \text{Tr}[\rho(t)\hat{n}(\mathbf{x})] = n(\mathbf{x}, t). \quad (\text{E8})$$

The coarse-grained ‘‘classical’’ density operator $\hat{n}_{(\text{cl})}(\mathbf{x})$ defined by $\mathcal{C}_\Lambda^{(\text{op})}$ has the property that, for density matrices that are diagonal in the smeared position basis at resolution Λ^{-1} , its expectation value coincides with $n(\mathbf{x}, t)$. The coherence density operator is then

$$\hat{n}_{(\text{coh})}(\mathbf{x}) = \hat{n}(\mathbf{x}) - \hat{n}_{(\text{cl})}(\mathbf{x}), \quad (\text{E9})$$

and its expectation value picks out the residual contribution from ρ_{off} .

In a representation where $\mathcal{C}_\Lambda^{(\text{op})}$ is implemented by smearing with a real, normalized kernel f_Λ , this expectation value can be written explicitly as

$$\langle \hat{n}_{(\text{coh})}(\mathbf{x}) \rangle_t \equiv n_{\text{coh}}(\mathbf{x}, t) = \int d^3x' f_\Lambda(\mathbf{x} - \mathbf{x}') \rho_{\text{off}}(\mathbf{x}, \mathbf{x}', t). \quad (\text{E10})$$

Here one may think of f_Λ as a Gaussian of width $\sim \Lambda^{-1}$, but the construction is general.

Similarly, the expectation value of the full spatial mass current is

$$\langle \hat{\mathbf{J}}(\mathbf{x}) \rangle_t = \frac{\hbar}{2mi} [\nabla_{\mathbf{x}'} \rho(\mathbf{x}, \mathbf{x}', t) - \nabla_{\mathbf{x}} \rho(\mathbf{x}, \mathbf{x}', t)]_{\mathbf{x}' = \mathbf{x}}. \quad (\text{E11})$$

Its coherence part, obtained from $\hat{\mathbf{J}}_{(\text{coh})} = \hat{\mathbf{J}} - \hat{\mathbf{J}}_{(\text{cl})}$, takes the form

$$\langle \hat{\mathbf{J}}_{(\text{coh})}(\mathbf{x}) \rangle_t \equiv \mathbf{J}_{\text{coh}}(\mathbf{x}, t) = \frac{\hbar}{2mi} \int d^3x' f_\Lambda(\mathbf{x} - \mathbf{x}') [\nabla_{\mathbf{x}'} \rho_{\text{off}}(\mathbf{x}, \mathbf{x}', t) - \nabla_{\mathbf{x}} \rho_{\text{off}}(\mathbf{x}, \mathbf{x}', t)]. \quad (\text{E12})$$

Equations (E10) and (E12) show that, for a single particle, the coherent part of the mass current is indeed a coarse-grained measure of the off-diagonal density matrix in the position basis. In particular, for a completely classical mixture ρ_{cl} diagonal in position at the resolution Λ^{-1} we have $\rho_{\text{off}} = 0$, and hence $n_{\text{coh}}(\mathbf{x}, t) = \mathbf{J}_{\text{coh}}(\mathbf{x}, t) = 0$, in agreement with the general operator statement $\text{Tr}[\rho_{\text{cl}} \hat{J}_{(\text{coh})}^\mu] = 0$.

2. Approximate continuity equation

Because $\hat{J}_{(\text{coh})}^\mu$ is exactly conserved as an operator, $\partial_\mu \hat{J}_{(\text{coh})}^\mu(x) = 0$, the expectation values $n_{\text{coh}}(\mathbf{x}, t)$ and $\mathbf{J}_{\text{coh}}(\mathbf{x}, t)$ obey an exact continuity equation,

$$\partial_t n_{\text{coh}}(\mathbf{x}, t) + \nabla \cdot \mathbf{J}_{\text{coh}}(\mathbf{x}, t) = 0, \quad (\text{E13})$$

for any state $\rho(t)$ evolving unitarily under the underlying Hamiltonian. In the single-particle, nonrelativistic

limit, this can also be verified directly by inserting the Schrödinger equation for $\rho(\mathbf{x}, \mathbf{x}', t)$ into Eqs. (E10)–(E12) and integrating by parts, up to boundary terms that vanish for localized wavepackets.

Collecting these results, we can define a coherence four-current

$$\mathbf{J}_{\text{coh}}^\mu(\mathbf{x}, t) = (c n_{\text{coh}}(\mathbf{x}, t), \mathbf{J}_{\text{coh}}(\mathbf{x}, t)), \quad (\text{E14})$$

which satisfies $\partial_\mu \mathbf{J}_{\text{coh}}^\mu = 0$ and is precisely the expectation value $\text{Tr}[\rho(t) \hat{\mathbf{J}}_{\text{(coh)}}^\mu(x)]$ in this single-particle sector. In this sense, the heuristic density-matrix formulas proposed in the phenomenological picture are not independent assumptions but concrete realizations of the general operator construction in a specific limit.

3. Effective nonrelativistic scalar potential

In the semiclassical regime where the hidden gauge field A_μ can be treated as a classical field sourced by the expectation value J_{coh}^μ , the $\mu = 0$ component A_0 plays the role of an effective scalar potential. The Maxwell-type equations of motion,

$$\partial_\nu F^{\mu\nu}(x) = g J_{\text{coh}}^\mu(x), \quad (\text{E15})$$

reduce, in a quasi-electrostatic approximation, to a wave equation for $A_0(\mathbf{x}, t)$,

$$\left(\nabla^2 - \frac{1}{c_L^2} \partial_t^2 \right) A_0(\mathbf{x}, t) = -g n_{\text{coh}}(\mathbf{x}, t), \quad (\text{E16})$$

where c_L is the propagation speed of the latent gauge field (equal to c in a relativistic completion).

For a single particle, the Schrödinger equation for ψ in the presence of A_0 can be written as

$$i\hbar \partial_t \psi(\mathbf{x}, t) = \left[-\frac{\hbar^2}{2m} \nabla^2 + V(\mathbf{x}) + gm A_0[\psi, \psi^*; \mathbf{x}, t] \right] \psi(\mathbf{x}, t), \quad (\text{E17})$$

where $A_0[\psi, \psi^*]$ is determined self-consistently by n_{coh} via the wave equation above. This makes explicit the statement that, in the nonrelativistic limit, the Quantum Latent Gauge interaction can be viewed as an effective, state-dependent scalar potential that is sourced only by the coherence structure of the state (encoded in n_{coh}) and vanishes for classical mixtures.

Appendix F: Phenomenological toy models in the nonrelativistic limit

The main text discusses experimental signatures of the Quantum Latent Gauge interaction in a fairly general setting. Here we present two simple, concrete nonrelativistic toy models that illustrate how the explicit formulas for n_{coh} and \mathbf{J}_{coh} translate into observable effects in interferometry and entanglement experiments.

1. Double-slit superposition and self-interaction

Consider a single particle in a one-dimensional double-slit-like superposition of two well-separated localized wavepackets,

$$|\psi\rangle = \alpha |L\rangle + \beta |R\rangle, \quad |\alpha|^2 + |\beta|^2 = 1, \quad (\text{F1})$$

where $|L\rangle$ and $|R\rangle$ are approximately orthogonal states localized near positions $x = \mp d/2$. In position representation,

$$\psi(x) = \alpha \phi_L(x) + \beta \phi_R(x), \quad (\text{F2})$$

with $\phi_{L,R}(x)$ normalized and weakly overlapping.

The density-matrix kernel is

$$\rho(x, x') = \psi(x) \psi^*(x') = \sum_{i,j=L,R} \alpha_i \alpha_j^* \phi_i(x) \phi_j^*(x'), \quad (\text{F3})$$

where $\alpha_L \equiv \alpha$, $\alpha_R \equiv \beta$. The diagonal part contains the classical probabilities $|\alpha|^2 |\phi_L(x)|^2$ and $|\beta|^2 |\phi_R(x)|^2$, while the off-diagonal part is

$$\rho_{\text{off}}(x, x') = \alpha\beta^* \phi_L(x) \phi_R^*(x') + \beta\alpha^* \phi_R(x) \phi_L^*(x'). \quad (\text{F4})$$

Substituting this into Eq. (E10) yields

$$\begin{aligned} n_{\text{coh}}(x) &= \int dx' f_\Lambda(x - x') \rho_{\text{off}}(x, x') \\ &= \alpha\beta^* \int dx' f_\Lambda(x - x') \phi_L(x) \phi_R^*(x') \\ &\quad + \beta\alpha^* \int dx' f_\Lambda(x - x') \phi_R(x) \phi_L^*(x'). \end{aligned} \quad (\text{F5})$$

If the slit separation d is comparable to or smaller than Λ^{-1} , the kernel f_Λ does not completely suppress the overlap between ϕ_L and ϕ_R , and $n_{\text{coh}}(x)$ is nonzero. In this regime the double-slit superposition sources a nontrivial latent gauge potential $A_0(x)$ via the quasi-static field equation.

In an interferometric geometry, the additional phase shift acquired due to the Quantum Latent Gauge self-interaction can be estimated by inserting the self-consistent $A_0(x, t)$ into the Schrödinger equation and integrating gmA_0/\hbar along each branch of the interferometer. To leading order in g^2 , and under mild symmetry assumptions, the result takes the form

$$\Delta\phi_{\text{QLG}} \sim g^2 \frac{m}{\hbar} T \mathcal{V} \mathcal{I}_{\text{geom}}, \quad (\text{F6})$$

where T is the interferometer time, $\mathcal{V} = 2|\alpha\beta|$ is the fringe visibility, and $\mathcal{I}_{\text{geom}}$ is a dimensionless integral encoding the spatial overlap of n_{coh} with the retarded Green's function of the latent field. This is consistent with the visibility-dependent phase shift discussed in Sec. III A of the main text, but now derived from an explicit nonrelativistic model.

2. Two-mode entanglement and coherence-selective coupling

As a second toy model, consider two distant spatial “qubits,” labeled 1 and 2, each realized as a particle in a double-well potential with localized basis states $|0\rangle$ and $|1\rangle$ (left/right). The Hilbert space factorizes as $\mathcal{H} = \mathcal{H}_1 \otimes \mathcal{H}_2$, with basis $\{|00\rangle, |01\rangle, |10\rangle, |11\rangle\}$. In this effective description, the coherence part of the mass current for qubit i can be represented (up to normalization and geometric factors) by an operator proportional to σ_i^x , since σ^x flips between the two localized wells and is sensitive to the off-diagonal element of the density matrix in the $\{|0\rangle, |1\rangle\}$ basis.

At leading order in g^2 , integrating out the latent gauge field in the Born approximation generates an effective interaction between the two qubits of the form

$$H_{\text{eff}}^{(12)} \propto g^2 m_1 m_2 \mathcal{K}(R) \sigma_1^x \sigma_2^x, \quad (\text{F7})$$

where m_i are the effective masses associated with each qubit, $\mathcal{K}(R)$ is a distance-dependent kernel obtained from the latent field propagator, and R is the separation between the qubits. Explicitly,

$$\mathcal{K}(R) \sim \int \frac{d^3 k}{(2\pi)^3} \frac{e^{i\mathbf{k}\cdot\mathbf{R}}}{\omega_k^2} [1 - W_\Lambda(\mathbf{k})]^2, \quad (\text{F8})$$

with ω_k the latent-field dispersion relation (e.g., $\omega_k = c|\mathbf{k}|$ for a massless mediator) and W_Λ the coarse-graining filter introduced in Sec. IID.

The expectation value of $H_{\text{eff}}^{(12)}$ in a joint state ρ_{12} is

proportional to $\langle \sigma_1^x \sigma_2^x \rangle$. For the Bell states

$$|\Phi^\pm\rangle = \frac{1}{\sqrt{2}}(|00\rangle \pm |11\rangle), \quad (\text{F9})$$

one finds $\langle \sigma_1^x \sigma_2^x \rangle = \pm 1$, whereas for a classical mixture

$$\rho_{\text{mix}} = \frac{1}{2}(|00\rangle\langle 00| + |11\rangle\langle 11|), \quad (\text{F10})$$

one obtains $\langle \sigma_1^x \sigma_2^x \rangle = 0$. Thus, the latent-gauge-induced coupling between the two qubits is entanglement-selective: it is nonzero only when the joint state contains genuine nonlocal coherence between the wells of the two systems.

This simple model makes concrete the qualitative statement in the main text that Quantum Latent Gauge predicts entanglement-dependent forces: for fixed local populations of each qubit, the presence or absence of spatial entanglement changes the effective interaction energy. In a realistic implementation (e.g., spatial qubits encoded in cold atoms, ions, or mechanical modes), one would have to include geometric factors, the full latent-field propagator, and environmental noise, but the essential feature—dependence on $\langle \sigma_1^x \sigma_2^x \rangle$ rather than on local densities alone—remains.

These nonrelativistic toy models thus provide a bridge between the rigorous operator-level framework of the main text and concrete experimental observables, and they show explicitly how the Quantum Latent Gauge interaction reduces, in simple limits, to the intuitive picture of a state-dependent scalar potential sourced only by quantum coherence.